RNA BIOLOGY
2026, VOL. 23, NO. 1, 1–24
https://doi.org/10.1080/15476286.2026.2690792

Taylor & Francis
by informa

RESEARCH ARTICLE

OPEN ACCESS Check for updates

The RNA binding protein ZFP36L2 displays tissue-selective mRNA targeting in mice

George Stephen Stephenson [a,b], Dalia Fleifel [a], Jeanette Gowen Cook [a], Alain Laederach [c,b,d] and Silvia Beatriz Vieira Ramos [a,d]

[a]Department of Biochemistry and Biophysics, University of North Carolina, Chapel Hill, NC, USA; [b]Bioinformatics and Computational Biology Program, University of North Carolina, Chapel Hill, NC, USA; [c]Biology Department, University of North Carolina, Chapel Hill, NC, USA; [d]RNA Discovery Center, University of North Carolina, Chapel Hill, NC, USA

ABSTRACT

ZFP36L2 (zinc finger protein 36 like 2, C3H type-ZFP) is an RNA-binding protein targeting transcripts rich in adenine-uridine elements (AREs). Previous transcriptomic analysis suggested that ZFP36L2 displays a distinct transcript preference or 'specific activity'. However, this analysis was restricted to a few tissues. Here, using experimental data in multiple tissues we detected a remarkable transcript selectivity depending on the tissue. Given that ZFP36L2 accelerates the degradation of specific ARE-transcripts upon binding, we obtained differential expression transcriptomic data on a Zfp36l2 knock-out mouse model to delve into the mechanisms governing this tissue-specific targeting. Transcriptomic analyzes of up-regulated ARE-transcripts in six tissues, lung, liver, bone marrow, spleen, kidney, and ovary of the Zfp36l2-deficient mouse confirmed that there is high tissue preference in ZFP36L2 targets. We observed only one common up-regulated gene, Apol11b, among these six different tissues. However, we do observe common trends, specifically an enrichment in protein coding genes in the up-regulated genes, consistent with these RBP primarily targeting genes on their 3' UTRs. Interestingly, we observed a significant increase in the proportion of IgV (immunoglobulin) genes being up-regulated. We further performed eCLIP (Enhanced Cross-Linking&ImmunoPreciptation) on a mouse cell line to explore potential binding sites of ZFP36L2. AU-Rich Element score (AREscore) analysis revealed enrichment in both up-regulated genes and eCLIP peaks, although some differences were observed in flanking residue composition. Our findings provide new insights into the intricate regulatory network orchestrated by ZFP36L2, opening avenues for exploring its potential roles in different tissues.

ARTICLE HISTORY
Revised 12 June 2026
Accepted 14 June 2026

KEYWORDS
Post-transcriptional gene expression; zinc finger protein 36 like 2; cell cycle; adenine uridine rich elements; RNA-binding protein

CONTACT Silvia Beatriz Vieira Ramos sramos@med.unc.edu Department of Biochemistry and Biophysics, University of North Carolina, Chapel Hill, NC, USA

Supplemental data for this article can be accessed online at https://doi.org/10.1080/15476286.2026.2690792

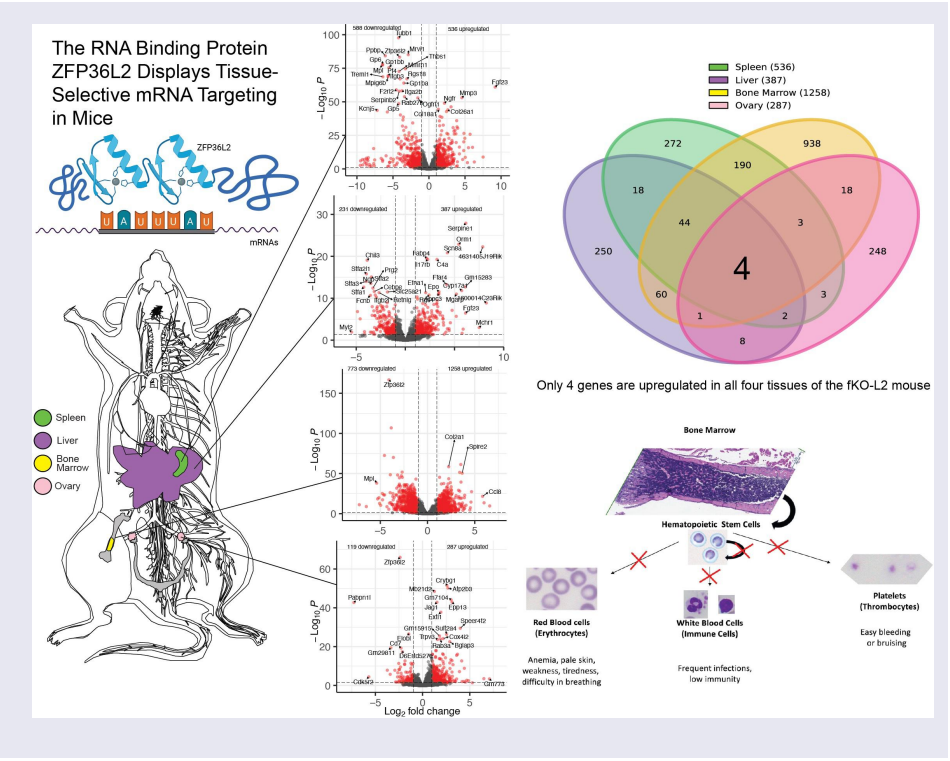

Background

The Zinc Finger Protein 36 Like 2 (ZFP36L2) belongs to the class of *adenine-uridine-rich element (ARE)-RNA binding proteins (ARE-RBPs)*. ARE-RBPs either stabilize or promote degradation of their target transcripts [1–4]. AREs comprise a variety of distinct adenine- and uridine-rich nucleotide sequences, typically located in the 3' UTRs of mRNAs that have relatively short half-lives [5,6]. The AUUUA pentamer is considered the minimum core motif, and AREs are subdivided in several classes [7,8] based on pentamer number and arrangement.

Although investigators have extensively identified specific binding sequences for RBPs, the consequences of the RNA/protein interactions are more difficult to assess. The tristetraprolin (TTP) family [9], or the zinc finger protein 36 (ZFP36) family, comprises a group of RBPs that interact directly with ARE-containing transcripts. Once the protein/RNA complex is formed, the most evident effect is to accelerate mRNA degradation by recruiting the CCR4/CAF1 deadenylases [10] and PABPC1 [11] in addition to decapping enzyme [12] and exosome.

Most studies of the ARE specificity of the ZFP36 family are focused on the prototypical family member, ZFP36 [12–14]; comparatively little is known about the specificity of the other two family members, ZFP36L1 and ZFP36L2. In the study described here, we focused on the specificity of ZFP36L2.

The ubiquitous expression of *Zfp36l2* mRNA in tissues/organs (GTEx RNA-seq data) suggests a range of yet to be evaluated functions of *Zfp36l2*. Particularly, the functions of ZFP36L2 in the lungs, liver, and kidney have not been adequately assessed, despite the association of many RBPs with diseases of these organs, such as ischaemic lung injury [15], chronic metabolic and inflammatory fatty liver diseases and cancer [16] and diabetic kidney [17]. Mouse models provided the first evidence for the importance of ZFP36L2. Disruption of the first of the two *Zfp36l2* exons resulted in viable animals. However, the females were infertile because of arrest of early embryo development at the 2-cell stage [18]. Interestingly, complete knockout of *Zfp36l2* resulted in premature death of homozygous pups by the end of the second week of life [19,20], likely due to anaemia consequent to haematopoietic stem cell defects. These initial functional role for ZFP36L2 in mouse, has also been confirmed in humans. More recently, Zheng et al. reported that expression of biallelic deleterious polymorphisms in the human *Zfp36l2* gene also leads to female infertility [21], and Iwanaga et al. found that acute leukaemia was associated with mutations in *Zfp36l2* [22]. While

other ARE-RBPs, such as TIAR and HuR, have been implicated in the chemotherapy resistance of haematologic malignancies [23].

Zhang et al. and Chousal et al. identified ZFP36L2-regulated mRNAs in erythrocyte lineage cells using an *ex vivo* knockdown [24] and an oocyte knockout model [25], respectively. Surprisingly, when we compared our splenic up-regulated gene dataset from *Zfp36l2*-fKO mouse [19] with these two datasets of genes up-regulated in the absence of ZFP36L2 we identified only one up-regulated genes in common to all three tissues. This single up-regulated gene overlap was in marked contrast to the approximate 7,000 expressed/detected genes in common among these three different tissues. Nevertheless, this result was obtained using three different biological models and distinct methodologies, microarray for the erythrocyte lineage, single cell RNA-seq (scRNA-seq) for oocytes and RNA-seq in spleen. These observations led us to hypothesize that ZFP36L2 has preferential mRNA targets depending on the tissue. If that is the case, ZFP36L2 would regulate distinct groups of genes depending on the tissue. To determine whether this apparent ZFP36L2 tissue preference was present in a range of tissues, here we used one biological model, our newly developed *Zfp36l2 flox* global knockout mouse model (L2-fKO) and the same methodology, RNA-seq, to obtain different tissue data sets. This mouse line, L2-fKO, lacking *Zfp36l2* in all tissues, was created by crossing the CMV-Cre mouse (Jackson Labs) with a *Zfp36l2-flox/flox* mice line, where exon 2 of *Zfp36l2* is flanked by *flox* sequences [19]. Six organs, lungs, liver, bone marrow, spleen, kidney and ovary were collected from experimental and control animal groups. RNA-seq data from all samples were analysed using a poly(A) library selection. The obtained results support our hypothesis that ZFP36L2 has distinct mRNA target preference depending on the tissue; only one up-regulated gene, *Apol11b*, was common to all tissues.

Results

Differential gene expression analysis in six mouse tissues

To identify potential ZFP36L2 mRNA targets, we performed differential gene expression analysis of RNA-seq data collected from six different mouse tissues from WT and L2-fKO pups, carrying and lacking both *Zfp36l2* alleles in all tissues, respectively, ages D6 to D9 post-birth. This developmental age was chosen, because these animals die during their second week of life as we reported previously due to haematopoietic defects [19,20]. We identified differentially expressed genes as having $\log_2|\text{Fold Change}| > 1$ and $p_{adj} < 0.05$. In Figure 1, in the left and right upper quadrants delineated by the red dotted lines in A to F, down-regulated genes are coloured in blue and up-regulated genes are in orange. Genes with a $\log_2|\text{Fold Change}| < 1$ or $p_{adj} > 0.05$ were classified as unchanged genes (grey). Data sets obtained for all tissues, satisfactorily clustered for the biological replicates in our RNA-seq data, based on the principal component analysis (PCA) and fold-change versus normalized mean counts (MA) plots as shown in Supplementary Figure S1A. To exclude that genes in the different organs are expressed in a sex-biased pattern in our samples, we performed PCA and MA analysis by sex in the liver (an organ where many genes are expressed in a sex-biased pattern) and observed no clustering by sex (Supplementary Figure S1B), suggesting no sex effect at that particular prepubertal age investigated. We classified coding and non-coding genes based on the protein coding annotations in Ensemble mouse (GRCm38). We chose the Ensemble annotations because they provide a coarse level of annotation, especially for non-coding genes. In the volcano plots and pie charts shown in Figure 1, we separated up-, down-, and unchanged genes into two sub-categories, coding (darker colours) and non-coding (lighter colours).

The fraction of coding vs. non-coding genes varied among tissues, as did the number of genes regulated. Ovary had the highest percent of non-coding regulated genes (Figure 1(F), 26.1% and 23.3% for down and up-regulated, respectively), whereas kidney (Figure 1(E), 10.5% and 5.8%) had the lowest. In general, for the down-regulated genes (blue), the percent of coding to non-coding was similar to the percent of coding to non-coding for unchanged genes (grey). In contrast, the percent of coding genes was more variable when we compared up-regulated coding genes (orange) vs unchanged genes. That is, in BM and kidney, the percent of coding genes (light orange) was greater compared with the unchanged genes, whereas the percent of coding genes was lower in the other tissues. Interestingly, the largest number of up-regulated coding genes was observed in bone marrow (1135) and spleen (430), which are tissues where haematopoiesis occurs at this development stage, D6 to D9

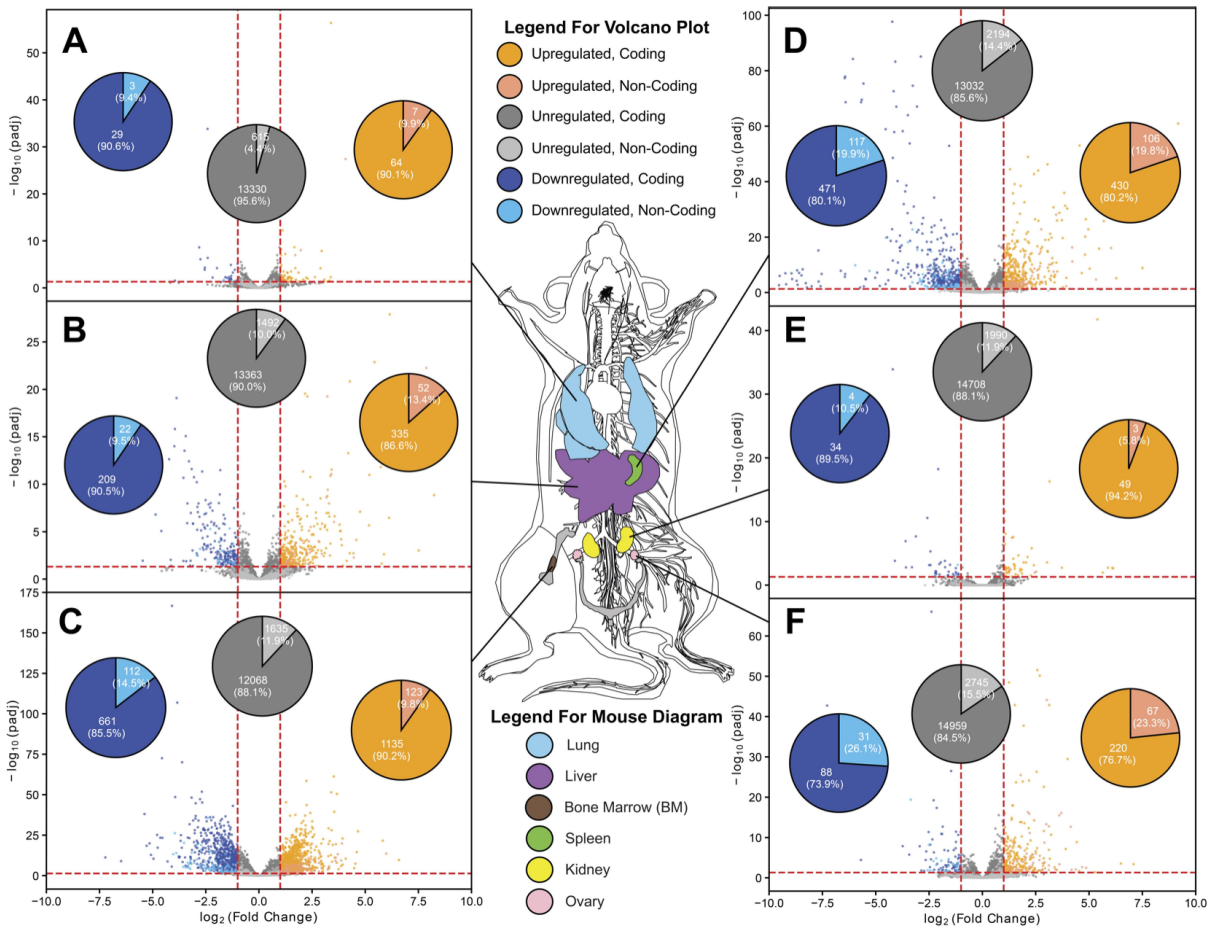

Figure 1. Differential gene analysis of *Zfp36l2* knockout mouse. We collected RNA sequencing data from six mouse tissues for both wild-type (WT) and *Zfp36l2* knockout mice. Down-regulated genes are colored in blue, up-regulated in orange, and unchanged in gray. The inset pie charts divide the gene sets as coding and non-coding. Genes with a $\log_2$(Fold change) > |1| and $p_{adj} < 0.05$ were considered differentially regulated in (A) lung, (B) liver, (C) bone marrow, (D) spleen, (E) kidney and (F) ovary.

post-birth. Possibly, the pancytopenia phenotype of the knockout mouse is a result of these up-regulated mRNAs that are normally targets for ZFP36L2. Interestingly, among all six tissues we analysed, bone marrow and spleen had the highest expression levels of *Zfp36l2*, 7000 and 6000 TPMs in the WT mice, respectively (Supplementary Figure S2A). To test if the increased or decreased number of targets in each of these tissues was likely due to the absence of *Zfp36l2* and not a potential compensatory effect of the other family members, we calculated the expression levels of *Zfp36* and *Zfp36l1* in all tissues analysed. In all the tissues, the other family members do not seem to compensate for the lack of *Zfp36l2*, except for the ovary where both *Zfp36l1* and *Zfp36* were slightly increased (Supplementary Figure S2B and C).

Gene annotation of differentially regulated genes

To identify trends common among the different tissues, we plot all genes (unchanged, down- and up-regulated) in a single volcano plot, where each gene was counted only once, in Figure 2(A). We observe that only in the up-regulated genes (light orange) there is a ~ 6.4% enrichment in protein coding genes relative to unchanged. Whereas we observed only a slight increase (1.5%) in coding genes that were down-regulated (dark blue). Thus, the absence of ZFP36L2 led to preferential upregulation of coding genes, suggesting that ZFP36L2 mainly downregulates coding sequence genes in the tissues studied.

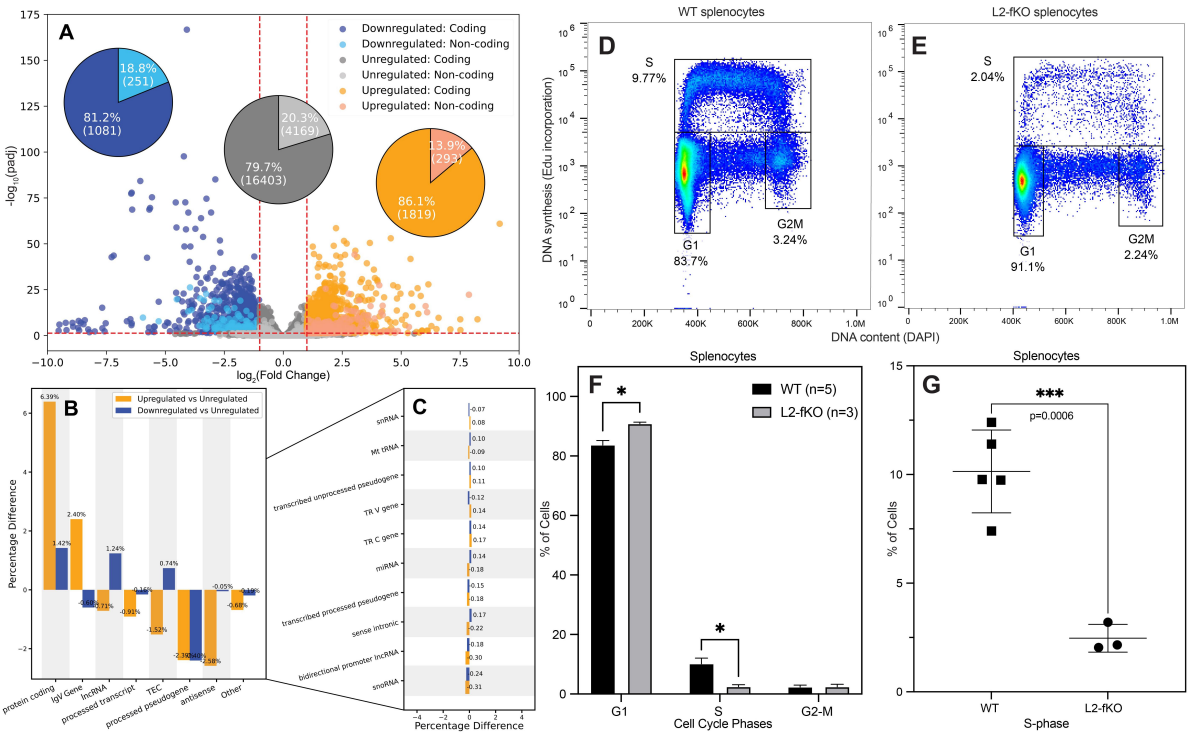

Figure 2. Differential gene analysis of *Zfp36l2* knockout mouse across all tissues and cell cycle progression in splenocytes. We combined our analysis across all six mouse tissues for both wild-type (WT) and *Zfp36l2* knockout animals. Down-regulated genes are colored in blue, up-regulated in orange, and unchanged in gray. The inset pie charts divide the genes by coding and non-coding. Genes with a $\log_2$(Fold change) > |1| and $p_{adj} < 0.05$ were considered differentially regulated. (A) Volcano plot of differential gene expression showing a general increase in the fraction of coding mRNAs in the up-regulated genes relative to non-coding and down-regulated gene sets, consistent with preferential targeting of 3′ UTRs by ZFP36L2. (B) Percent change in gene type annotations (as per RefSeq gene annotations) for up- and down-regulated genes in all six tissues. There was a 6.4% increase in the fraction of coding genes in the up-regulated set (relative to unchanged), whereas in the down-regulated set there was a 1.5% relative increase. Similarly, IgV genes (immunoglobulin variable regions) were overrepresented in the up-regulated gene set. Conversely, long non-coding RNAs were overrepresented in down-regulated genes but underrepresented in up-regulated genes. (C) RefSeq annotations include additional "other" categories, none of which are significantly over- or under-represented in the differential gene expression analysis. (D) WT and (E) KO representative samples of isolated splenocytes were assessed for EdU incorporation and DNA content by flow cytometry, after a 60 min exposure to EdU *ex vivo*. Both animals were of the same age, D8 post birth, and from the same litter. (F) Percent of cells in each cell cycle phase, G1, S and G2-M are illustrated. Samples were analyzed using FlowJo software. An ANOVA test was used to determine significance for multiple samples (*$p = 0.01$). (G) Comparison of cells from WT ($n = 5$) and L2-fKO ($n = 3$) animals in S-phase using a t test for comparing two samples (***$p = 0.0006$).

To better understand whether there was a major change in any gene category of up- or down-regulated, we calculated the percent difference between up-regulated vs. unchanged genes (Figure 2(B), orange) and down-regulated vs unchanged genes (Figure 2(B), blue). As mentioned earlier, the Ensemble-specific annotation of mouse genes was used for this categorization. When we subdivided the genes, it became clear that most up-regulated genes were protein coding genes, i.e. mRNAs. Additionally, among the protein coding genes, the immunoglobulin variable (IgV) genes comprised a relatively high percent of up-regulated genes, 2.40%; thus, the IgV genes are represented in their own category (Figure 2(B)). The immunoglobulin variable genes encode the variable portion of the immunoglobulin chains, and they generate diversity and specificity of the immunoglobulins. Long non-coding RNAs (lncRNAs, containing or not containing introns) and processed pseudogenes lacking introns that are thought to arise from retrotransposition were underrepresented in the up-regulated category. 'To be Experimentally Confirmed' genes, i.e. genes with poly (A) features but which are not experimentally validated, were slightly underrepresented in the up-regulated group and overrepresented in the down-regulated group. All other gene categories had minor variations (Figure 2(C)).

Because IgV genes are only expressed in B cells, and the spleen is the primary site for maturation of early B cell populations during D5-D9 post-birth, we decided to isolate splenocytes from WT and L2-fKO and assess their proliferation by measuring EdU incorporation. EdU is a thymidine analog that is incorporated into DNA by cells undergoing active DNA replication. In the spleen, the B cells are activated and undergo rapid proliferation along with differentiation into plasma cells and memory cells, that then exit the spleen. Note that B cells are one component of the heterogeneous cell types that compose the spleen. However, because we used polysucrose density gradient centrifugation to first remove most red cells, debris and other cell types, our 'splenocytes' were enriched for immune cells including monocytes and lymphocytes, in particular B cells. Surprisingly, the L2-fKO 'splenocytes' had nearly 5-fold reduction in S phase population (Figure 2(E and G)), with a correlating increase in G1/G0 (Figure 2(F)). The G1 phase is a critical stage for B cell differentiation because during this period, B cells receive signals that trigger their activation and subsequent differentiation into either memory B cells or plasma cells.

Overlap of up-regulated genes and gene ontology analysis

As mentioned, ZFP36L2 binds AU-rich elements in 3' UTRs, and this interaction results in RNA degradation. Thus, the up-regulated genes in the knockout mice are of particular importance to our analysis. Our previous transcriptomic analysis raised the idea that ZFP36L2 display a distinct tissue targeting specificity [19]. As mentioned earlier, when we performed a similar analysis using previously published data [24,25] in early burst-forming unit-erythroid and oocyte, respectively, and spleen in our knockout, we found a single common gene that did not have an ARE [19]. However, this low overlap could be due to different biological models and use distinct methodologies, thus justifying the present investigation using the same biological model and methods. Here we perform an overlap analysis on our new experimentally obtained data sets to identify genes up-regulated in multiple tissues and test our idea that ZFP36L2 has preferential mRNA targets depending on the tissue. This analysis is illustrated in Figure 3(A) as an upset plot. Strikingly, only a single gene, apolipoprotein L 11b (*Apol11b*), was up-regulated in all six tissues (S1 in Figure 3(A and E)). To answer if the up-regulated genes were equally detected among all tissues, we analysed the expression of all up-regulated genes in each specific tissue by obtaining the mean TPM values from WT animals (Supplementary Table 1). The up-regulated genes are detected in each tissue at similarly high percentage rates, varying from 74% to 83% (Supplementary Table S2). This suggests that up-regulated genes in each tissue are not uniquely expressed in each tissue, but rather up-regulated in specific tissues. Additionally, only few genes that were uniquely up-regulated (Figure 3(A) on the right) are present solely in that tissue (Suplementary Table S3), except for ovary. Thus, most genes that were uniquely up-regulated in one tissue are expressed in all tissues but only up-regulated in that one.

Only 17 genes (listed in Figure 3(E)) were up-regulated in four or more tissues (subsets S1-S8 in Figure 3(A)) of a total of 10,887 genes present in common, less than 0.1%. Notably, the three tissues with the highest number of up-regulated genes in common are liver, spleen and bone marrow; tissues where ZFP36L2 has a known role *in vivo*, in immuno-haematopoiesis [19,20,24,26,27]. The largest number of shared up-regulated genes, 184, was in spleen and bone marrow. Again, this finding likely reflected the fact that both tissues have haematopoietic functions at this developmental age, and that the KO phenotype, pancytopenia, revels potential ZFP36L2 targets in those organs.

To identify potential biological processes, cellular components, or molecular functions significantly overrepresented, we performed a Gene Ontology enrichment analysis of up-regulated genes present in more than three tissues (Figure 3(B)), two tissues, (Figure 3(C)), and only common to spleen and bone marrow (Figure 3(D)). This analysis identified some common terms, such as 'response to Type II interferon' and 'cell killing' (Figure 3(B)) and 'lymphocyte mediated immunity' (Figures 3(C and D)). These terms likely reflected the haematologic defect of pancytopenia observed in the L2-fKO, as well as cellular stress responses resultant from the phenotype. In addition, 'immune system process' and cellular response, such as 'signaling receptor activity' and 'response to stimulus' were overrepresented (darker blue) in most of the 17 genes up-regulated in four or more tissues (Figure 3(E)). Similarly, for genes up-regulated in two tissues (Figure 3(C)), the enriched GO terms were also related to immune functions, so that they provided little clarification of specific pathways or molecular processes modulated by *Zfp36l2*.

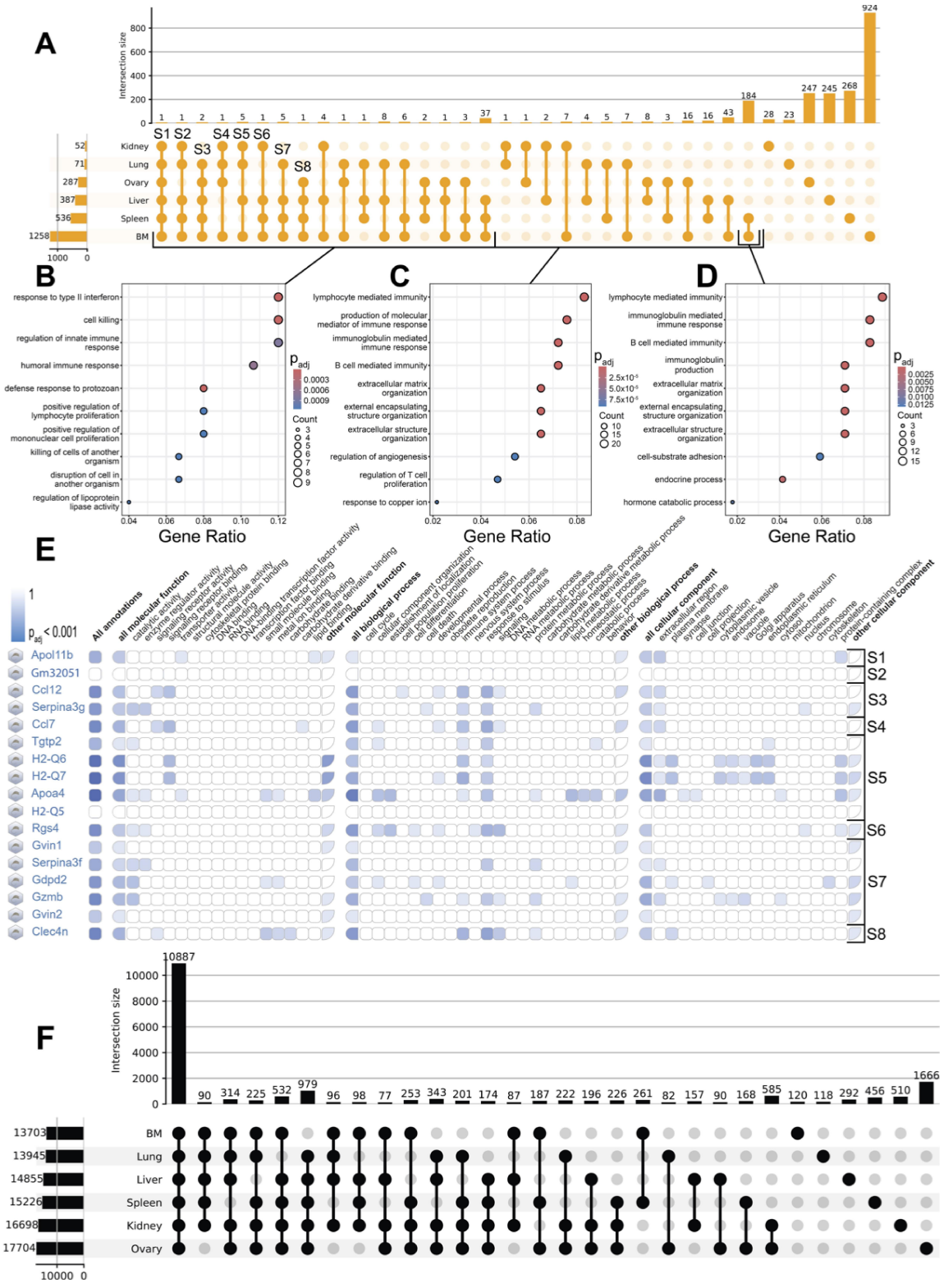

Figure 3. Overlap and Gene Ontology analysis of up-regulated genes in *Zfp36l2* knockout tissues. (A) Upset plot of up-regulated genes in six tissues. Only one gene, *Apol11b*, was up-regulated in all six tissues (subset S1). The genes simultaneously up-regulated in four or more tissues are labeled S1-S8, and their respective names are shown in E. Three up-regulated genes (subsets S2, S3) were common to five tissues, and 13 genes were upregulated in common in four tissues (subsets S4–S8). However, most of the up-regulated genes were upregulated in only one tissue, indicating an extensive tissue-selectivity targeting of ZFP36L2. (B) Gene Ontology analysis of up-regulated genes in three or more tissues. (C) Gene Ontology analysis of up-regulated genes in two tissues. (D) Gene Ontology analysis of up-regulated genes in bone marrow and spleen. The overrepresented terms in B, C, and D are mostly related to immune response. (E) ribbon diagrams of GO terms for up-regulated genes in four or more tissues, organized by common sets. (F) upset plot of unchanged genes in six tissues and their tissue distribution, confirming that most of the genes were detectable in the RNA-seq of all six tissues.

To provide a more robust way to compare independently derived gene expression data sets, we also performed GeneOverlap [28] analysis (Supplementary Figure S4A) followed by a Gene Set Enrichment Analysis (GSEA) to identify potential *common pathways* modulated by the lack of *Zfp36l2*. The GSEA for each tissue in a rank-ordered list is summarized in an upset plot (Supplementary Figure S4B) and listed as a heatmap of hallmark pathways (Supplementary Figure S4C). No single pathway was significantly enriched in all six tissues. However, inflammatory pathways such as TNF-α and IL6 were significantly enriched in 5 out of 6 tissues (Supplementary Figure S4B and C, coloured in green), although in bone marrow they were negatively enriched. Additionally, five other inflammatory pathways (inflammatory response, IL2-Stat5 signalling, allograft rejection, IFN-α and IFN-γ responses, Supplementary Figure S4B and S4C, coloured in purple) were significantly enriched in liver, kidney, lung and ovary, but not in spleen and bone marrow. Overall, liver had the highest number of significantly enriched pathways (20, with Z-score >1), followed by kidney [16], lung [15], ovary [12], bone marrow [9], and spleen [1]. Likely, the predominance of inflammatory pathways observed in the L2-fKO mouse is a consequence of the decreased number of all white blood cells. These findings are consistent with our GO analysis where 'immune system process' and cellular response, such as 'signaling receptor activity' and 'response to stimulus' were overrepresented (Figure 3(E)). Finally, other significantly enriched pathways were observed only in some specific tissues, for example 'epithelial mesenchymal transition' in liver and bone marrow, as well as 'mTORC1 signaling' strongly represented in spleen.

It is important to compare the up-regulated upset plot in Figure 3(A) with the same analysis for the unchanged genes shown in Figure 3(F). Approximately 70% of all unchanged genes (10,887/~15,000genes Figure 3(F)) were expressed in all six tissues. In contrast 0.04% (1/2,583) of up-regulated genes were found in all tissues. Thus, we would expect far greater overlap in the differentially regulated genes than what was observed in Figure 3(A). We also performed a similar analysis of down-regulated genes (Supplementary Figure S3). *Zfp36l2* was found among the down-regulated genes in all six tissues, confirming the lack of this gene in the L2-fKO mouse model as expected.

The contrasting overlap analysis of up-regulated genes (Figure 3(A)) versus unchanged genes (Figure 3(F)) suggested that the genes uniquely up-regulated in each tissue would be genes most likely to reveal specific organ functions regulated by ZFP36L2. Thus, we performed GO enrichment analysis of up-regulated genes in each tissue (Figure 4). The GO analysis in each tissue revealed functions and biological processes related to the physiology of the tissue itself. This result was not necessarily surprising because each gene set was uniquely up-regulated in an individual tissue. For example, for the liver (Figure 4(B)), after the inflammatory genes common to all tissues, we observed that there was a category of genes affected by a lack of *Zfp36L2* which were related to the catabolic and metabolic function of this organ, such as 'NADH regeneration' and 'glucose catabolic process to pyruvate'. In fact, nearly the entire glycolytic pathway from glucose-6-phosphate to pyruvate was de-repressed in the knockout (*Gpi1*, *Pfkl*, *Pfkp*, *Aldoa*, *Tpi1*, *Gapdh*, *Pgk1*, *Pgam1*, *Eno1* and *Pkm*; log2 fold change +1.1 to +2.8, all padj <0.05), accompanied by the lactate exporter *Slc16a3* (MCT4) and the hypoxia regulators *Egln3* and *Ddit4*, suggesting that ZFP36L2 normally restrains a glycolytic, lactate-exporting program in the liver. Whereas in the bone marrow (Figure 4(C), Table 1), the up-regulated genes were related to the bone marrow environmental niche and the extracellular matrix that are required for proper differentiation of stem cells into each differential blood cell type.

Overall, some trends emerged from the GO analysis. Most of the common terms reflected genes related to immune system function, such as response to type II interferon (lungs), regulation of T cell activation (liver), collagen-containing extracellular matrix (bone marrow), immunoglobulin-mediated immune response (spleen), antigen processing and presentation of exogenous peptide antigen (kidney), and cytokine-mediated signalling (ovary). To distinguish the organ-specific signal from the immune terms common to these largely immune-related tissues, we separated GO terms that recurred across tissues from those enriched in a single tissue (Table 1). The shared terms were dominated by generic immune and chemotaxis processes, whereas the tissue-specific terms reflected the characteristic physiology of each organ, including glycolysis in liver, skeletal and connective-tissue development in bone marrow, xenobiotic glucuronidation in kidney, triglyceride and lipid handling in lung, and meiotic germ-cell programs in ovary. Therefore, the overall analysis suggested that ZFP36L2 likely regulates not only different immune pathways in general but also genes related to the physiology of each organ.

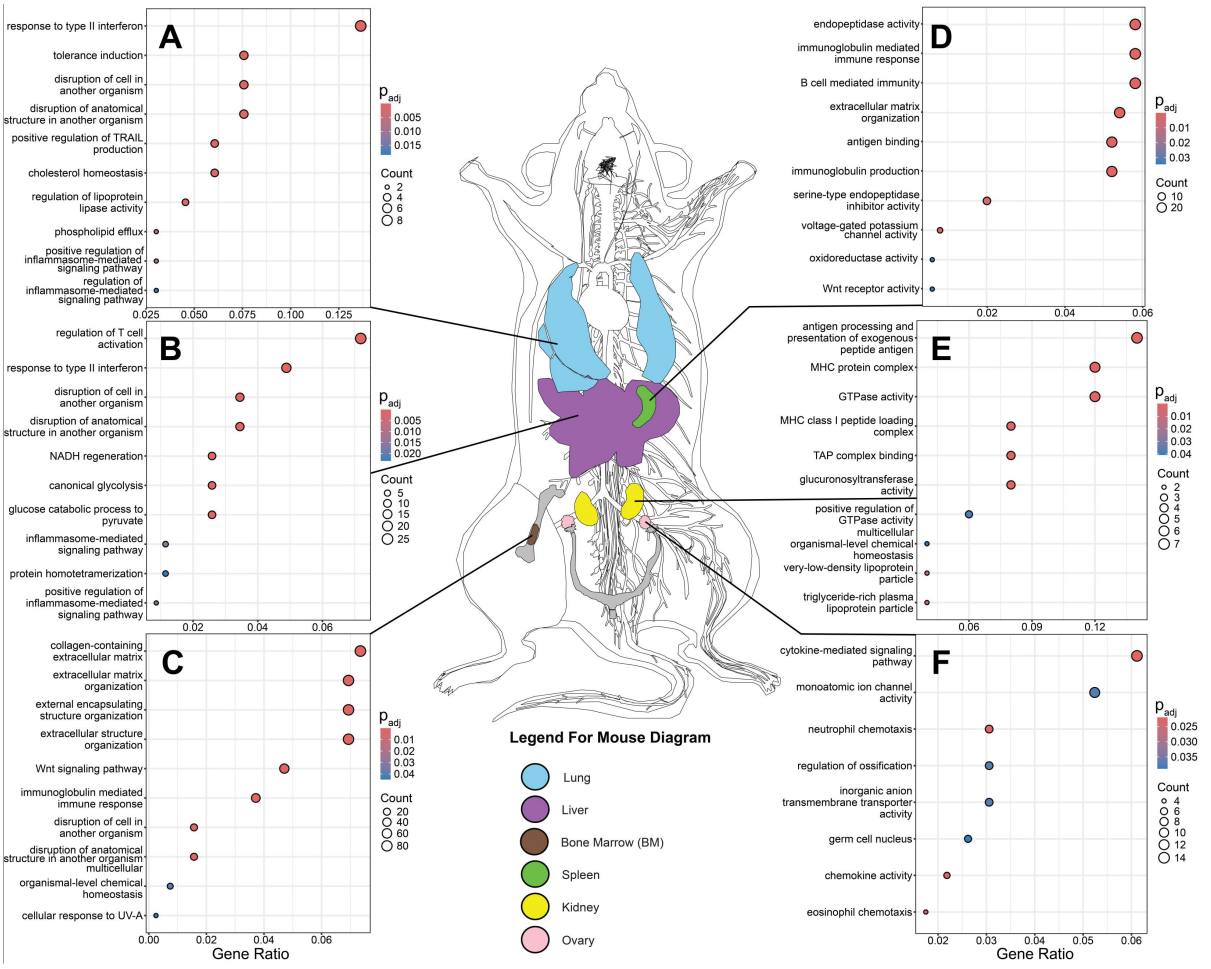

Figure 4. Gene Ontology analysis of up-regulated genes in each tissue. We performed Gene Ontology enrichment analysis on genes uniquely up-regulated in each tissue to identify enriched terms specific to each tissue. We selected terms with $p_{adj} < 0.05$ and gene enrichment ratio > 0.01. The GO terms identified for A) lung, B) liver, C) bone marrow, D) spleen, E) kidney and F) ovary.

Table 1. Gene ontology enriched terms, once immune terms common to multiple tissues are excluded.

Tissue	Distinctive (non-shared) gene program — representative terms and genes
Liver	Glycolysis / NADH regeneration / glucose-to-pyruvate (*Gpi1*, *Pfkl*, *Pfkp*, *Aldoa*, *Tpi1*, *Gapdh*, *Pgk1*, *Pgam1*, *Eno1*, *Pkm*)
Bone marrow	Bone, cartilage and connective-tissue development; biomineralization (*Col1a1*, *Col2a1*, *Bmp7*, *Sp7*, *Mmp13*, *Fgfr2*)
Kidney	Xenobiotic glucuronidation: glucuronosyl-/UDP-glycosyltransferase activity (*Ugt1a9*, *Ugt1a10*, *Ugt3a1*, *Ugt3a2*)
Lung	Triglyceride / lipid metabolism, lipase inhibition (*Apoc3*, *Angptl3*, *Apoa4*, *Sik1*)
Ovary	Meiosis / germ cell: synaptonemal complex, germ-cell nucleus (*Sycp3*, *Fkbp6*, *Morc1*, *Tbpl2*, *Lhx8*)
Spleen	Vascular (VEGF-response) and ion-channel regulation (*Pik3cb*, *Emilin1*, *Kcnq1*, *Kcne3/Kcne4*)

The only gene up-regulated in all six tissues was *Apol11b*, thus we further test if there was a direct interaction of ZFP36L2 protein and this transcript. This gene is predicted to enable chloride channel action and lipid binding activity, but the specific function remains to be determined. In all six L2-fKO tissues, *Apol11b* had higher RNA-seq read depth in the knockout (Figure 5(A)). In most WT tissues, *Apol11b* was expressed at low levels, except for spleen and bone marrow (Figure 5(B)). *Apol11b* has only one ARE, a 7-mer type (UAUUUAU), in its 3' UTR, 73 nucleotides downstream of the stop codon. To determine whether ZFP36L2 directly binds to *Apol11b* mRNA, we synthesized an RNA probe that included this ARE and performed a gel shift assay. ZFP36L2 clearly bound to *Apol11b* (Figure 5(C)). Another family member, ZFP36, apparently did not bind, whereas ZFP36L1 bound weakly (Figure 5(D)). Immunoblotting showed that all ZFP36 family members were present at comparable levels in the protein extracts used for the gel

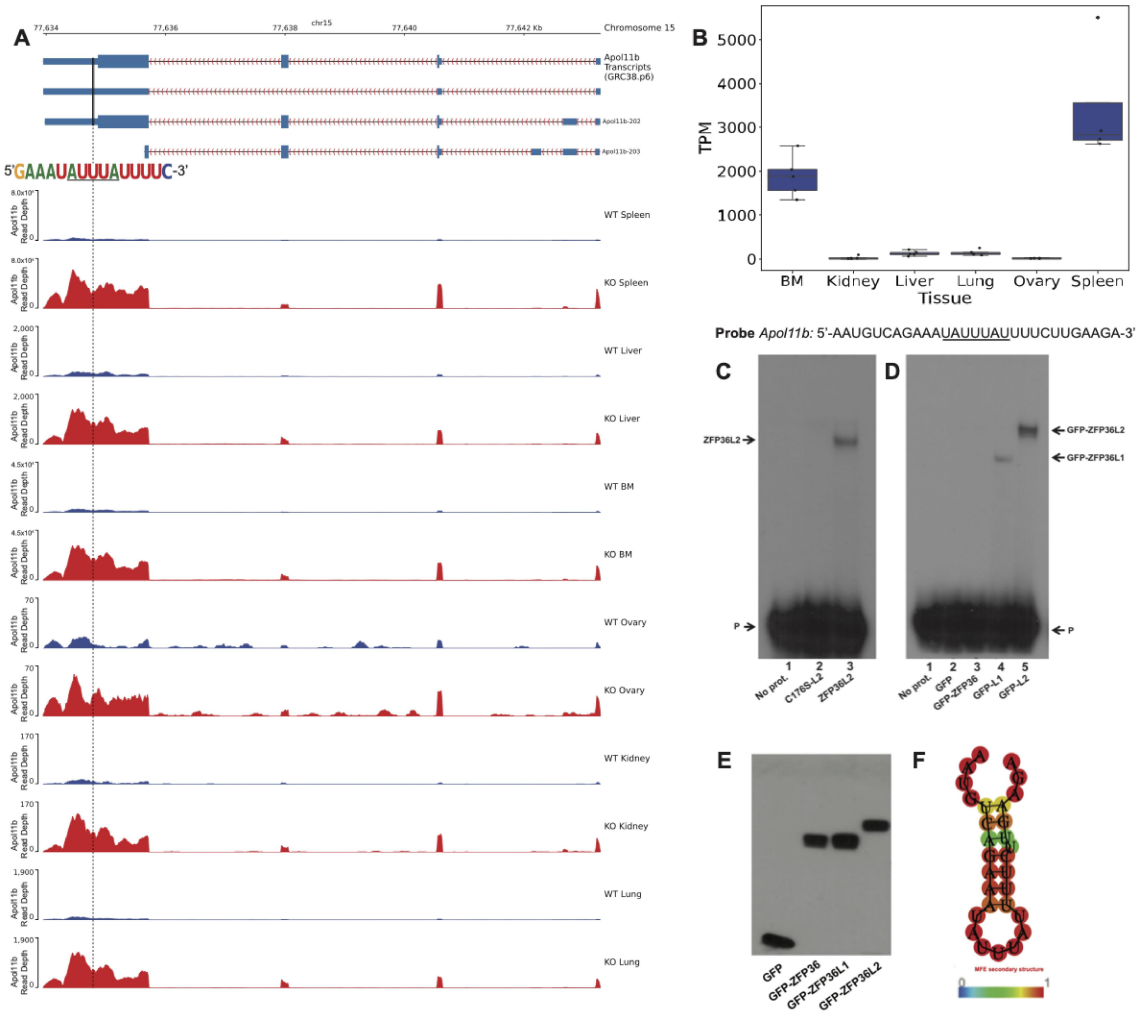

Figure 5. *Apol11b*, the only gene up-regulated in all six tested tissues. (A) Upper panel shows the four transcript variants of *Apol11b*. Lower panel shows coverage plots for *Apol11b* from RNA-seq results. RNA-seq coverage for WT is shown in blue, and KO is shown in red; black dashed bars indicate the location of the 7-mer ARE in the 3′ UTR. The pattern of read depth coverage is similar in all tissues, suggesting no change in relative transcript isoform abundance, but instead an overall change in gene expression. (B) Expression of *Apol11b* across WT tissues based on transcript per million (TPM) obtained by RNA-seq. (C) RNA electrophoretic mobility shift assays were performed by incubating 10 µg of protein extract from HEK 293 cells transfected with ZFP36L2-C176S (lane 2) or ZFP36L2 (lanes 3) constructs with *Apol11b* probe. Lane 2 corresponds to a mutation (mC176S) in the first mZFD that abrogates binding. (D) EMSA performed by incubating 10 µg of protein extract from HEK 293 cells transfected with GFP (lane 2) or with vectors expressing the GFP-ZFP36 proteins with *Apol11b* probe. The sequence of the *Apol11b* mouse probe, 29 nt, is shown above the EMSA. (E) Immunoblotting of protein extracts used in the EMSA in panel D were probed with GFP-antibody. Five µg of protein extracts were loaded per lane. (F) Secondary structure prediction for the *Apol11b* probe using RNAfold web server. The color-code scale shown at the bottom is for the prediction confidence for each base pair in the structural model.

shift assay (Figure 5(E)). These results suggested that *Apol11b* is a specific mRNA target of ZFP36L2, although ZFP36L1 had a lower affinity for this transcript. In the present *in vivo* model, *Zfp36l1* expression is not increased in any KO tissue, except for a modest increase in the ovary (Supplementary Figure S2B), thus ZFP36L1 is unable to compensate for the effect of ZFP36L2 in controlling *Apol11b in vivo*. Interestingly, an RNAfold analysis of the 29-nt *Apol11b* probe predicted that the ARE was within a loop (Figure 5(F)) resembling the structure we obtained for the functional ARE in the LHR transcript using SHAPE-Map [29].

AU-rich element analysis of regulated genes

Because ZFP36L2 binds to adenine-uridine-rich elements (ARE) within the 3 'UTRs of mRNAs, we used the ARE*Score* algorithm to analyse the sequences of the 3' UTRs of up- and down-regulated genes. This algorithm is based on quantifying three typical features of AREs: the number of 'AUUUA' pentamer motifs, the proximity between the pentamers, and the presence of AU content surrounding the pentamer [30]. A high ARE*Score* indicates a high likelihood that the 3' UTR is a target of the ZFP36 family of proteins. When we compared the ARE*Scores* from the up-regulated genes (Figure 6(A), orange, mean 3.75) with the down-regulated genes (Figure 6(A), blue, mean 2.82) from all six tissues combined, the mean score was clearly greater for the up-regulated set (****$p = 1.48 \times 10^{-12}$). Thus, the 3' UTRs of up-regulated genes preferentially contain ARE sequences likely to bind ZFP36L2. Additionally, when we performed a similar analysis for each tissue individually (Figure 6(B)), the ARE*Scores* for up-regulated genes were also significantly greater for each tissue, except for lung and ovary. Note that the largest difference in ARE*Score* was for bone marrow ($p = 1.55 \times 10^{-5}$) and liver ($p = 3.58 \times 10^{-5}$). ARE*Score* did not correlate with the number of tissues in which a gene was up-regulated (Spearman $\rho = -0.03$, $p = 0.17$), consistent with the predominantly tissue-restricted response in which 82% of up-regulated genes were uniquely up-regulated in a single tissue. Notably, tissue-specific up-regulated genes carried ARE*Scores* comparable to broadly-regulated genes and significantly higher than downregulated genes (mean 3.97 vs 2.96, $p = 3 \times 10^{-9}$), indicating that the ARE Score enrichment is a pervasive feature of the up-regulated population rather than a property of a few consistently regulated genes. In contrast, the ARE*Scores* in up-regulated non-coding genes were not increased in comparison to the down-regulated genes (Supplementary Figure S5). In fact, the mean of ARE*scores* in non-coding up-regulated genes was significantly lower than ARE*scores* in down-regulated non-coding genes. Most of the long non-coding genes are nuclear [31], whereas ZFP36L2 is mainly cytosolic with shuttling properties [32]. These findings, support our results presented in Figure 2(A), suggesting that ZFP36L2 does not seem to modulate non-coding genes in our mouse model.

We performed position weight matrix (PWM) analysis of the flanking sequences of 5-mer AREs in the 3' UTRs of up-regulated genes for each tissue individually (Figure 6(C)). Uridine was the flanking nucleotide with the highest probability adjacent to the core 5-mer AUUUA motif in all tissues. This result was consistent with our previous work that showed the minimum binding requirement of ZFP36L2 to be a 7-mer UAUUUAU motif [19]. Although some differences in ARE flanking PWMs were observed across tissues, the differences were small.

Interaction of ZFP36L2 with the transcriptome

The transcriptome includes all RNA transcripts expressed in each cell type at a specific time or in a particular condition. Based on the results in Figure 2(B), we concluded that ZFP36L2 tends to target mRNAs that have protein coding sequences, i.e. open reading frames. To determine whether ZFP36L2 tends to regulate mRNAs high or low expressed in each tissue, we obtained the expression values in transcripts per million (TPMs) for all the genes captured by our RNA-seq. The up-regulated genes had a 6-fold decrease in expression levels in comparison to down-regulated genes (TPM ~100 vs TPM ~600, respectively, ****$p < 0.00005$), Supplementary Figure S6A, suggesting that ZFP36L2 preferentially targets mRNAs that are expressed at low levels in mouse tissues.

To explore mRNA sequences directly bound to ZFP36L2, we performed duplicate enhanced UV cross-linking followed by immunoprecipitation experiments with an anti-ZFP36L2 antibody (eCLIP); a rabbit IgG was used as negative control. Other investigators have performed eCLIP experiments with ZFP36L2, however those studies were conducted only in human cell lines [27] and never using murine lines. Because the 3' UTRs are not well conserved, in contrast to 5' UTRs that tend to be conserved in evolution, we deemed it necessary to collect murine-specific binding data to test how they overlapped with our up-regulated data set. Initially, we attempted these experiments in primary bone marrow cells from WT pups at D7 to D9 post-birth because that period precedes the initial phenotypic signs observed in the L2-fKO animals. However, these samples did not pass IP quality controls, and we had to resort to an established mouse culture cell line. To explore that we used MLTC-1 cells because, previously, we detected endogenous ZFP36L2 by immunoblotting in these cells [29,33]. MLTC-1 is a Leydig cell line derived from the mouse

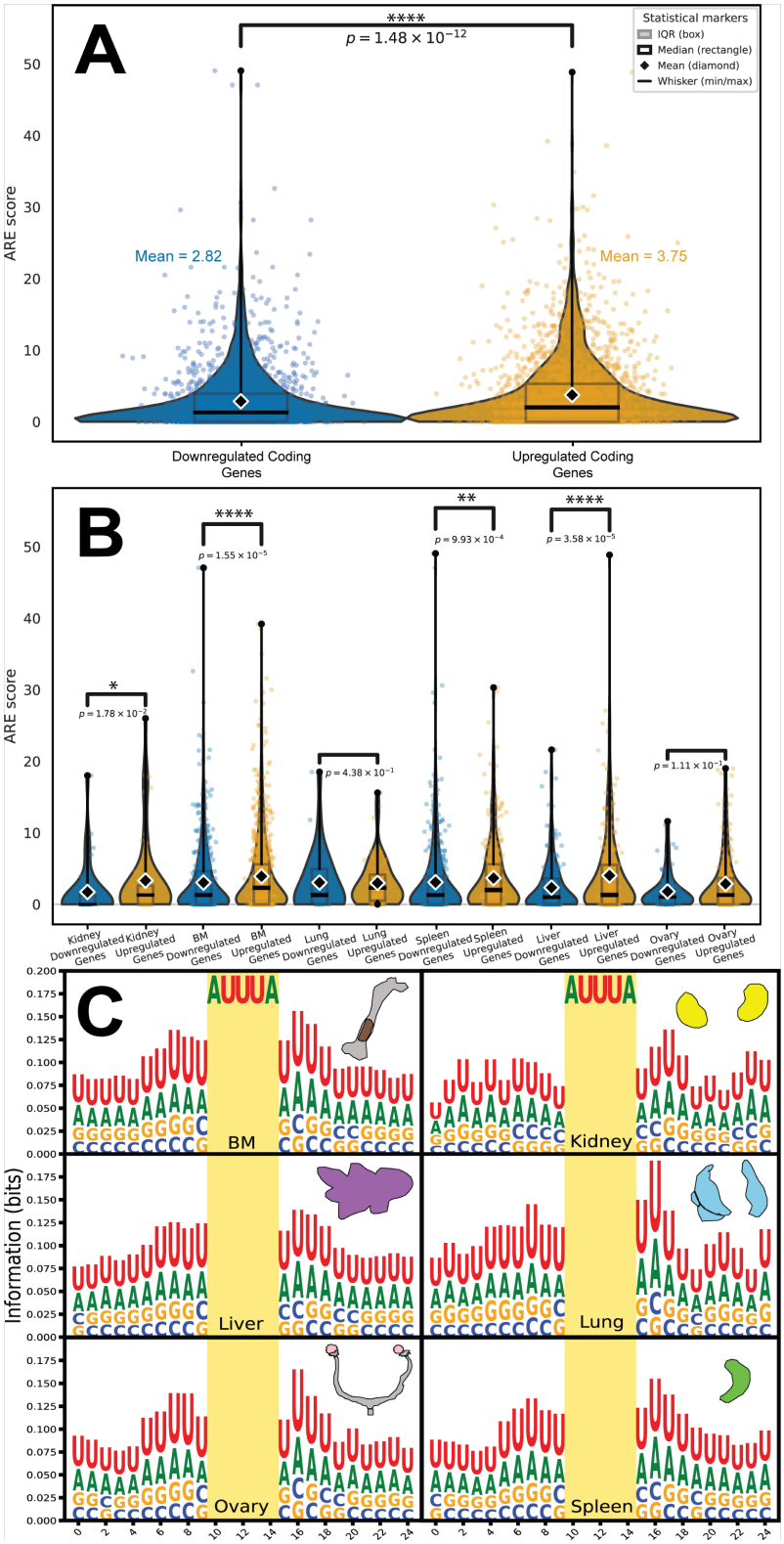

Figure 6. ARE analysis of 3′ UTRs in differentially regulated genes. (A) ARE*Score* analysis of all coding gene 3′ UTRs for up- (orange) and down- (blue) regulated genes. The mean ARE*Score* of up-regulated genes was greater compared with down-regulated genes (3.75 vs 2.82, $p = 1.48 \times 10^{-12}$, using a traditional two-tailed t-test). (B) A greater ARE*Score* was also observed in up-regulated genes in most individual tissue, consistent with the fact that ZFP36L2 preferentially binds AREs. (C) Motif analysis of the sequences flanking the AREs in the 3′ UTRs of up-regulated genes. In each individual tissue, there was a common flanking U predominance.

testis, thus raising the question if this would be a limitation of performing eCLIP in these cells to compare with our RNA-seq data. To address that we checked how many genes are expressed in common between our RNA-seq from all six tissues and a recent RNA-seq from MLTC-1 cells [34]. Most of the genes, 68%, captured in our RNA-seq from mouse tissue overlap with genes expressed in MLTC-1 cells (Supplementary Figure S7), whereas only 13% are expressed exclusively in MLTC-1 cells.

We identified 2,143 eCLIP sequences with $\log_2$(Fold Change) >1 and $\log_{10}$(p) <1. These peaks mapped to 597 different genes. To explore how these findings could be interpreted in the context of our mouse model, we intersected up-regulated genes in each tissue with these 597 eCLIP genes (Figure 7(A)). We noticed that the highest intersection occurred with bone marrow, i.e. 34 genes. Liver was second with 10 genes, and

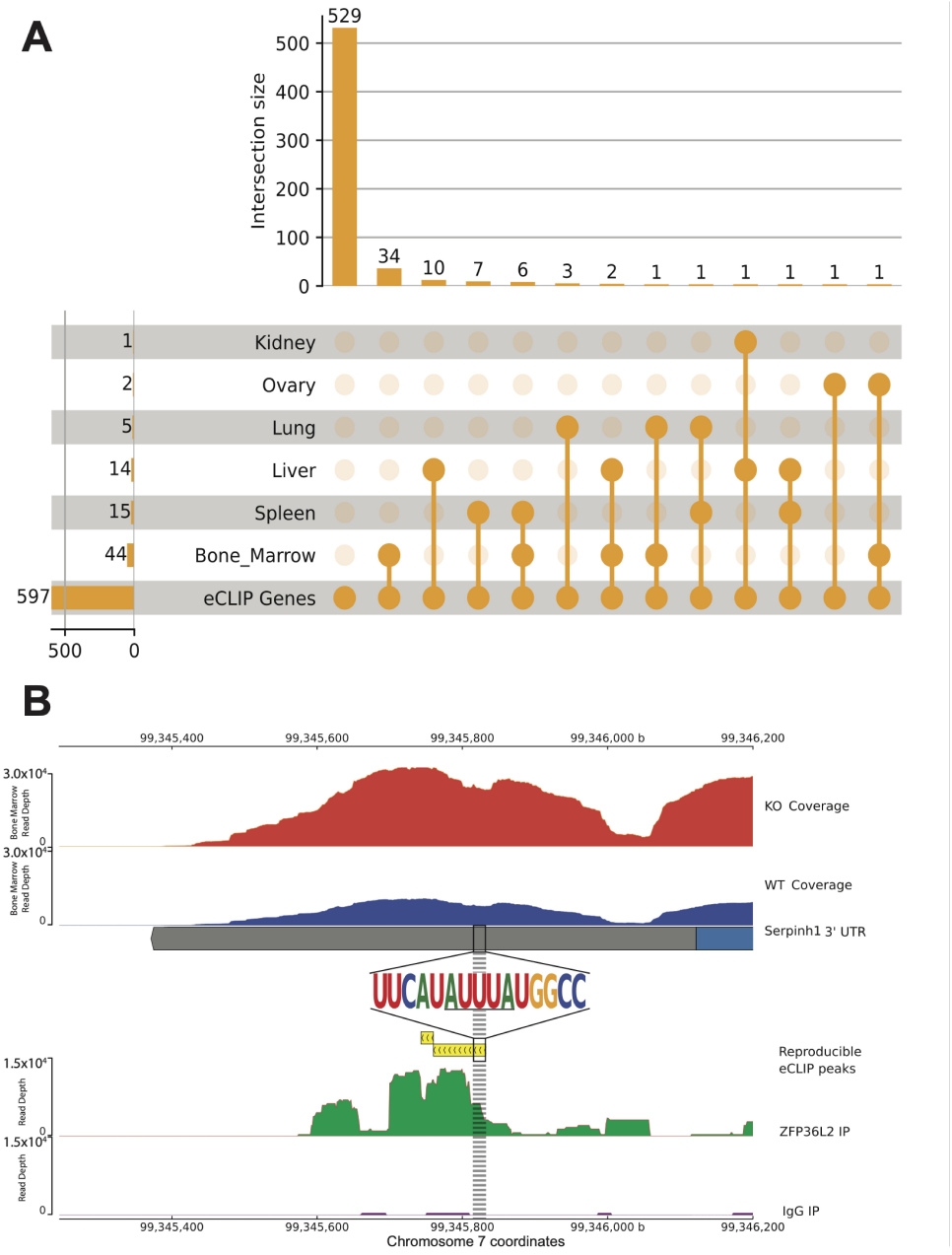

Figure 7. Intersection of up-regulated genes and eCLIP peaks. (A) Upset plot of genes in which at least one ZFP36L2 eCLIP peak present in both eCLIP duplicate samples from MLTC-1 cells was present in the 3′ UTR and in the set of up-regulated genes from each tissue. (B) Genomic track of 3′ UTR of *Serpinh1*, a gene up-regulated in bone marrow. RNA-seq results show higher coverage plot in the KO (red) versus the WT condition (blue). The lower panel shows raw ZFP36L2 IP in green compared with the IgG control in purple. The reproducible eCLIP peaks (across two conditions) are shown as yellow rectangles. One 7-mer ARE is present at the 5′ end of the first eCLIP peak.

spleen was third with 7 genes. Notably, these three organs are important sites of haematopoiesis during the early development stage of D6 to D9 post-birth, the period when we collected samples for RNA-seq. Of note, overall, eCLIP peaks captured by the specific antibody were derived from genes expressed at a higher TPM (>3,000) (Supplementary Figure S6B).

To exemplify how these intersections of up-regulated and eCLIP sequences looked in our raw data, we chose one representative gene, *Serpinh1*, up-regulated in bone marrow (Figure 7(B)). The upper panel of Figure 7(B) illustrates the 3' UTR coverage obtained by RNA-seq for the L2-fKO condition (red) compared with WT (blue). There was significantly greater read depth of the 3' UTR in the KO, consequently *Serpinh1* was classified as an up-regulated gene in the bone marrow. In the lower panel, we plotted the window of one reproducible eCLIP peak (present in both IP data sets, yellow) found in *Serpinh1* (green). Interestingly, the black dashed bar corresponds one UAUUUAU motif. The lower panel of Figure 7(B) shows evidence for strong enrichment of the ZFP36L2 IP track (green) when we compared the data with the IgG IP control (purple), resulting in the peak call. In Supplementary Figure S8 we show coverage tracks for four additional representative bone marrow genes, *Col4a1, Fstl1, Lox, and Lpl*. We chose these four genes because they had at least one ARE of the 5-mer type (AUUUA) in 3' UTR. A flanking motif analysis around the AREs in eCLIP peaks showed an enrichment for uridines surrounding the AREs (Supplementary Figure S8E). Whereas a *de novo* motif analysis using HOMER found three of the six first ranked motifs, as being U enriched motifs. This U enrichment is particularly visible in motif #5 (Supplementary Figure S9).

Expression of the mRNA-degradation machinery in the Zfp36l2 knockout

Because ZFP36L2 acts as a sequence-specific adaptor that recruits the general mRNA-decay machinery to ARE-containing transcripts rather than degrading RNA itself, the up-regulation of target mRNAs in the knockout could in principle arise from changes in the levels of the degradation enzymes. To test this, we examined the differential expression of 115 genes spanning the mRNA-degradation machinery across all six tissues (Supplementary Figure S10): the catalytic and structural core of decay (Supplementary Figure S10A), its activators and adaptors (Supplementary Figure S10B), and the sequence-specific RNA-binding proteins that recruit the machinery to specific mRNAs (Supplementary Figure S10C). The catalytic machinery was essentially unchanged in the knockout: across the 71 detected core genes the changes were small (median per-gene maximal $|\log2FC| \approx 0.34$), and only *Noct* and *Patl2* reached significance with $|\log2FC| \geq 1$, each in a single tissue and in opposite directions, with no coordinated regulation of any decay module. By contrast, and as expected, *Zfp36l2* was the most strongly and consistently down-regulated gene of the entire set (log2FC −1.85 to −4.09; all padj <0.05), confirming the knockout, and the few additional changes were largely restricted to the recruiter layer (for example, the paralog *Zfp36* in bone marrow). These results indicate that de-repression of ARE-containing targets in the *Zfp36l2* knockout reflects loss of ZFP36L2-mediated recruitment of an intact degradation machinery rather than a change in the abundance of the degradation enzymes.

Discussion

RNA-binding proteins (RBPs) are associated with liver, kidney, and lung diseases. In the liver, 92 RBPs are up-regulated in hepatocellular carcinoma [35]. Members of a prominent class of RBPs, to which ZFP36L2 belongs, the adenine-uridine-rich element (ARE)-binding proteins (ARE-RBPs), are involved in chronic metabolic and inflammatory fatty liver diseases and cancer [16,36]. Other ARE-RBPs are associated with hypoxia-response signalling in kidney epithelial cells [37], diabetic kidney disease [17], and protection from ischaemic lung injury [15]. Despite the associations of ARE-RBPs with liver, kidney, and lung disorders, the mechanism(s) by which these RBPs contribute to disease are unclear. To determine whether ZFP36L2 has mRNA tissue preference and uncover the function of this protein in organs not previously investigated, we analysed potential mRNA targets of ZFP36L2 in different tissues, using our newly developed *Zfp36l2 flox* global knockout mouse model (L2-fKO). The goal of our investigation was to define the mechanism and 'rules' that favour tissue-specific function of ZFP36L2, an ARE-RBP. Knowing that upon binding, ZFP36L2 accelerates the degradation of specific ARE-containing transcripts, we expect that target genes would be up-regulated in the L2-fKO animals. To identify these transcripts, we obtained differential expression

transcriptomic data from lung, liver, bone marrow, spleen, kidney, and ovary. We found multiple transcripts up-regulated in each of these tissues as expected. However, there was a notable transcript selectivity of ZFP36L2 according to tissue even though most genes are expressed in all six tissues (Figure 3 and Supplementary Table 2). Only one up-regulated gene, *Apol11b*, was commonly up-regulated in the six different tissues investigated, suggesting that ZFP36L2 selectively targets different mRNAs in different tissues. Other alternative explanations would include (a) tissue-specific expression of target mRNAs (i.e. the gene is not expressed in some tissues, so cannot be regulated), (b) differential ARE accessibility due to secondary structure or competing RBPs, and (c) functional compensation by ZFP36L1 or ZFP36. ARE accessibility would require obtaining RNA secondary structure data for example using SHAPE-map and direct competition of ZFP36L2 with other RBPs, which are beyond the scope of our current investigation using our mouse model, thus cannot be excluded. However, the data presented here does not support possibilities (a) and (c). In Supplementary Table S1 (under GSE283043) we showed that the up-regulated genes are detected in each tissue at similarly high percentage rates, varying from 74% to 83%, tissues. Except for ovary, only few genes that were uniquely up-regulated are present solely in that tissue (Suplementary Table S3). These results suggest that up-regulated genes are expressed in all tissues but only up-regulated in that one, talking against possibility (a). To investigate functional compensation, possibility (c), we measure measured *Zfp36* and *Zfp36l1* expression in all six tissues (Supplementary Figure S2) and found no major compensation except in ovary. Another compensatory mechanism would be differences in mRNA-degradation machinery, which does not seem to be the case, given that the catalytic machinery was essentially unchanged in the knockout (Supplementary Figure S10).

Despite this observed tissue selectivity of ZFP36L2 in choosing its mRNA targets in a particular tissue, we observed common trends. First, we clearly noticed that most of the up-regulated genes were coding genes, confirming at the transcriptomic level that ZFP36L2 preferentially modulates protein coding mRNAs. Second, ARE*scores* were significantly increased only in up-regulated genes but not in down-regulated genes. This increase in ARE*scores* was particularly evident in bone marrow, spleen and liver, which are haematopoietic organs at the early developmental age investigated here. Similarly, when ZFP36L2 was knocked down in a primary erythroid cell lineage [24] and knocked out in oocytes [], ARE*Scores* were increased in the up-regulated genes. The ARE*Score* algorithm was developed and optimized for ZFP36 [30]. The wide use of ARE*Score* confirmed its usefulness for detecting potential targets of other ZFP36 family members. Although some differences in ARE flanking PWMs were observed across tissues, the differences were small, suggesting that the tissue specificity of up-regulated genes is modulated by factors other than specific sequence motifs recognized by the tandem zinc finger domain of ZFP36L2. Third, when identifying common pathways in multiple tissues in up-regulated genes using Gene Ontology and GSEA we found terms related to immune system processes, response to stimulus and inflammatory pathways. Whereas genes uniquely up-regulated in a single tissue tended to be related to functions and biological processes particular to the physiology of that tissue.

Surprisingly, among the coding genes modulated by ZFP36L2 the IgV genes were overrepresented (Figure 2). The IgV genes are unique to B cells, they encode the variable regions of antibodies, the domains that determine the uniqueness of an antibody. Notably, IgV genes undergo an extensive V(D)J recombination in B cells. V(D)J recombination is a process of somatic gene rearrangement unique to lymphocytes where variable (V), diversity (D), and joining (J) gene segments are recombined by the activity of the recombination activating genes (RAG). This recombination leads to an increased somatic hypermutation (SHM) rate with significant gene instability in germinal centre B cells. Thus, we hypothesize that ZFP36L2 can influence SHM in B cells, what would require investigation of DNA mutation or hypermutation in these cells. Future gene instability assays and DNA sequencing data in L2-fKO B cells will be necessary to investigate the mechanism by which ZFP36L2 contributes to genome stability or other DNA damage response (DDR). Other ARE-RBPs, such as AUF1, HuR, KHSRP, TIA-1, TIAR, including ZFP36L2, have been implicated in preserving genome stability by regulating DNA damage response [38].

In addition to this connection between ZFP36L2 and gene instability, we observed a cell cycle effect in B cells from the L2-fKO animals. These cells were arrested in G1 (or G0) of the cell cycle and very few cells entered in S phase when ZFP36L2 was absent. This finding supports our hypothesis that lack of ZFP36L2 affects DNA damage in splenic L2-fKO B cells. Note that Somatic hypermutation (SHM) is intrinsically linked to the B cell cycle, with high-rate mutagenesis restricted primarily to the G0/G1 phases. Interestingly,

Galloway et al. observed that in pro-B cells, ZFP36L1 and ZFP36L2 are critical for cell cycle before B cells are mature and express Ig receptors in the cell surface. They proposed that both RBPs suppress mRNAs whose protein products cooperatively promote transition to the S phase of the cell cycle [39]. Recently [40], reported that the dKO of ZFP36L1 and ZFP36L2 results in G2/M arrest due to accumulation of DNA damage in S phase [40], as opposed to our observed G1 arrest as a result of L2-fKO. In our study, we used enriched B cells from an *in vivo* system, whereas in [40], they used an *in vitro* GC B cell culture system. It is possible that dKO of both ZFP36L1 and L2 in an *in vitro* system will result in different cell cycle effects compared to the *in vivo* single ZFP36L2-KO performed in our study. While they observed cell cycle-related genes such as *Cdkn1a, Ccnd2, Ccne2, Cep76*, *Mdm2*, *Csnk1e, Nup88*, and *Ska2* increased in the dKO, none of these eight genes were captured in our eCLIP experiments. However, 11 other cell cycle-related genes were captured in our list of 2,143 eCLIP reproducible peaks, but none of them contained the minimal binding sequence for ZFP36L2, an ARE of the 7-mer type (UAUUUAU) suggesting an indirect control of ZFP36L2 on the cell cycle genes rather a direct binding. Only future studies may help clarify the underlying reasons for these variations. Additionally, in other biological models, ZFP36L2 has been implicated in directly modulating genes involved in terminal differentiation of other haematopoietic cell types, such as erythroid [24] and myeloid [27] cells, pointing to a progenitor defect in haematopoietic stem cells (HSC). The present work shows that ZFP36L2 affects B cell proliferation, which we suspect is not a cell-autonomous effect given that the up-regulation of IgV genes is only correlative.

The analysis of overlap among up-regulated genes in multiple tissues revealed only one common gene, *Apol11b*. We confirmed that ZFP36L2 interacts with the 3' UTR of *Apol11b* using gel-shift assays, but surprisingly this gene was not captured in our eCLIP data set. When we performed our eCLIP experiments we anticipated that even though MLTC-1 cells were unrelated to most tissues studied here, most genes would be commonly expressed. We confirmed that, given that approximately 70% of the genes expressed in these cells were simultaneously detected in the RNA-seq from all six mouse tissues (Supplementary Figure S7). However, there was still a possibility that *Apol11b* was not expressed in MLTC-1 cells. In fact, this is the case, *Apol11b* was not detected on a recent MTLC-1 RNA-seq [34], which we now confirmed by qPCR (not shown). This illustrates one of the main restrictions of eCLIP, it captures only genes expressed in the cell line it was performed, which may not reflect the same genes expressed in primary tissues. Therefore, some other hits captured in our RNA-seq can still be good candidates for direct ZFP36L2 target. Potentially, eCLIP experiments performed in a primary cell line, such as splenocytes, would overcome this limitation. Potentially, using splenocytes which are enriched in B cells would also clarify if ZFP36L2 directly interact with IgV genes. Additionally, we would like to pinpoint that eCLIP itself has its own limitations. One of them being that eCLIP does not capture all transcripts containing a consensus recognition for a given protein. Other groups have observed that this is the case for Unkempt, an RBP containing a cluster of CCCH-type zinc finger domains [41,42]. The reasons why, can be attributed to fragments of RNA captured that do not correspond to the short sequence involved in the direct binding. These could be considered false positive signals captured by the crosslinking between other domains of the protein that are in proximity with the RNA but are not directly mediating the binding. Aiming to increase the quality of eCLIP generated data, novel advances have been recently introduced, such as Size-Matched Input (SIM) improved library preparations and better bioinformatics pipelines [43,44]. Undoubtedly, the incorporation of footprinting SHAPE with eCLIP to identify nucleobases that are precisely hydrogen bound to the protein is one of the most promising advances to directly detect potential RNA consensus recognition sequence and RBPs [45]. Also extremely promising is the combination of non-isotopic ligation induced by UV crosslink and IP followed by mass spec [46]. Because of the intrinsic eCLIP limitations mentioned above, electrophoretic mobility shift assay (EMSA) was the alternative we employed to test the interaction of ZFP36L2 with *Apol11b* transcript. Given that *Apol11b* was significantly increased in multiple L2-fKO tissues and our EMSA showed a robust binding of ZFP36L2 to *Apol11b*, collectively we concluded that *Apol11b* is an *in vivo* target of ZFP36L2.

When we performed a flanking motif analysis around the AREs captured by eCLIP peaks, an enrichment for uridines surrounding the AREs (Supplementary Figure S8E) was noticed, which was similar to the results when we used the up-regulated genes combined (Figure 6(C)). Consistent with that, when we applied a *de novo* motif analysis using HOMER to find specific nucleotide sequences recognized by the tandem zinc finger domain of ZFP36L2, we found three of the six first ranked motifs are U-enriched motifs, particularly

in motif #5, UUUAUGC, (Supplementary Figure S9). Intriguingly, certain eCLIP peaks in our data did not contain a canonical AUUUA motif. Our observation was consistent with other ZFP36L2 eCLIP datasets using human cell lines [27], raising the possibility that ZFP36L2 binding is mediated by factors other than solely the presence of an ARE sequence motif. In summary, most eCLIP peaks tended to be uridine-rich, consistent with the analysis of sequences flanking ARE in the 3' UTRs of up-regulated genes (Supplemental Figures S8E and S9) but our eCLIP data did not captured the classic ARE 7-mer consensus recognition sequence (UAUUUAU). Maybe the presence of other RNA-binding proteins or miRNAs interacting with sequences in the 3' UTRs obscured our eCLIP detection. For example, the RBP ELAVL2 shares some ARE-RNA targets with ZFP36L2 [19] thus, potentially they compete for the binding to the same ARE sequence. However, we did not design this study to exclude these possibilities, but only to investigate potential ZFP36L2 targets.

Around 10% of our eCLIP peaks simultaneously overlap with up-regulated genes indicating some agreement between these two orthogonal approaches, however one would expect greater overlap. We suspect that the smaller than expected overlap was related to the inability of eCLIP, in this particular case, to detect genes expressed at low levels. Most of the up-regulated transcripts had TPMs below 200, which is considered a low level of expression. Whereas most eCLIP peaks captured in our experiments had TPMs above 1000. This corresponds to one order of magnitude difference in the expression levels using these different experimental approaches (Supplementary Figure S6), potentially explaining the smaller than expected overlap between eCLIP and up-regulated genes. Because of that, only highly expressed ZFP36L2 targets were likely to be detected by eCLIP. Thus, in our case, the combination of RNA-seq and eCLIP is still useful but perhaps too stringent to broadly uncover transcripts targeted by ZFP36L2, particularly because they tend to be expressed at low levels. These unexpected results demonstrate an underappreciated complication of integrating differential gene analysis with eCLIP data. However, the 57 genes from eCLIP that overlap with up-regulated genes in tissues relevant for haematopoiesis identified deserve further careful investigation. Once binding to ZFP36L2 is confirmed and consequent RNA degradation, these genes may shed light in understanding myelodysplastic syndrome in children, a rare disease that happens in four out of one million births and has been limitedly investigated.

Conclusions

Among all RNA binding proteins that recognize adenine-uridine rich elements, ZFP36L2 plays a unique and vital role in RNA metabolism, as it is required for normal haematopoiesis. Here, by investigating potential ZFP36L2-mRNA targets in multiple tissues, we provide a new understanding into the intricate regulatory network orchestrated by ZFP36L2, opening avenues for testing distinct RNA decay functions of ZFP36L2 according to its tissue environment. Additionally, our results demonstrate an underappreciated complication of integrating differential gene analysis with eCLIP data.

Material and methods

Mouse model and sample collection

We followed the ARRIVE 2.0 guidelines to report our animal experiments. Conditional *Zfp36l2* knockout mice carrying loxP sites flanking exon 2 of *Zfp36l2* (*Zfp36l2*$^{fl/fl}$) were crossed with B6.CTg(CMV-Cre)1Cgn/J (stock#006054) mice from Jackson Laboratory to generate animals with *Zfp36l2* alleles floxed as described [19]. These animals are referred to as L2-fKO or KO; they lacked *Zfp36l2* in all tissues from the early embryo stage onward. In both groups, WT and L2-fKO, were distinguished based on genotyping as previously described in [19]. Animals carrying both wild-type copies of *Zfp36l2* (WT) were used as controls. To minimize any potential confounders associated with development stage and sex, the collected tissues were derived from age-matched animals (D6 to D9 post-birth) of both sexes. In most collections, the WT and KO animal pairs were derived from the same litter aiming to minimize environmental or gestational effects. Thus, it was decided *a priori* that the animals to be included in the study had to be age-matched and derived from the same litter. Based on these criteria, even if a WT and a KO were from the same matched age but were born from a different litter, they were excluded and we did not collect samples. No randomization was used given that all

collected samples were included. Only the person who genotyped the animas was aware of the group allocation, further conducted experiments, outcome and data analysis were performed blindingly. The primary outcome measured was genes differentially regulated and cell cycle analysis performed in both groups. Traditional two-tailed t-test was used for analysis. Carbon dioxide (CO2) inhalation was the method of euthanasia used for mice, followed by cervical dislocation. Forty-six samples were collected from 23 pairs of animals, three for lung, five for liver, five for bone marrow, four for spleen, three for kidney, and three for ovary. Immediately after death, tissues were rapidly collected, in less than 10–15 min and total RNA was extracted. For each tissue collected, the independent replicates clustered in a PCA and the variability for both groups is summarized in Supplementary Figure S1. The tissues were collected from animals on days 6 to 9, i.e. at a short window post-birth and reflecting a similar developmental stage (except for one ovarian sample collected at D13). The samples were collected at that age because the KO animals die before they are 2 weeks old, likely due to a severe pancytopenia of the blood cells. Animals were housed in the Dental School vivarium of the UNC School of Medicine, Chapel Hill. The Institutional Animal Care and Use Committee of the University of North Carolina approved all animal experimentation (IACUC ID# 24–004).

RNA sequencing and data analysis

Total cellular RNA was freshly extracted from dissected mouse tissues using RNeasy plus (Qiagen) and quantified using a NanoDrop spectrophotometer (ThermoFisher). Three micrograms of total RNA from each sample treated with DNase (TurboDNA-free kit, Invitrogen) for 60 min. The total RNA was re-measured, and 2000 ng of DNase-treated RNA was submitted to Azenta Life Science for RNASeq. All 46 samples passed QC with RNA Integrity Numbers (RIN) >6 (average 9.2 ± 1.02) and RNA fragments >200 of 70% or higher. The DNase-treated RNA samples were then used to prepare a library using a poly(A) selection.

RNA sequencing was performed using an Illumina HiSeq platform by Azenta Life Science; the total yield was 388,685,940 reads. Each sample, representing a specific tissue, yielded an average of 35–60 million reads. Initial quality control involved using Trimmomatic v.0.36 to trim potential adapter sequences and low-quality nucleotides.

For alignment, STAR aligner v.2.5.2b was used, and reads were mapped to the Mus musculus ENSEMBL GRCm38 reference genome. Specifically, we used a two-pass mapping strategy in STAR. In the first pass, STAR was used to generate a database of splice junctions from the unannotated data. This database was then incorporated into the second pass, resulting in improved alignment accuracy for the entire read sequences. Additionally, parameters were optimized for sensitive detection of splice junctions, including setting –outSAMstrandField intronMotif and – alignIntronMin 20—alignIntronMax 500,000. More than 97.5% of the trimmed reads mapped to the reference genome.

Unique gene hit counts were subsequently determined using featureCounts from the Subread package v.1.5.2. Because of the strand-specific nature of the library, only unique reads mapping within exon regions were counted, maintaining strand specificity.

Differential gene expression analysis was conducted using DESeq2. A direct comparison between wild-type and L2-fKO samples was performed. The Wald test was used to calculate *p*-values and log2 fold changes. Genes were considered differentially expressed if they exhibited an adjusted *p*-value below 0.05 and an absolute $\log_2$ fold change exceeding 1.

We downloaded 3' UTR sequences from the NCBI Biomart [47] and analysed the longest sequence for each gene. The ARE*Score* program [30] was used to compute the AREscores for all 3' UTRs and then analysed for the up-regulated and down-regulated genes [30]. We compared mean AREScores using a traditional two-tailed t-test.

Splenocyte isolation

The entire spleen was dissected from five WT and three KO Day 8 pups. Studied animals were from the same litter. Any adipose tissue was trimmed away from the organ, and the spleen was placed on a 40-μ Nylon mesh filter in a 35-mm petri dish. Once the spleen was finely pressed through the filter mesh, the round haematopoietic cells moved through easily, whereas the stromal vascular fraction remained on the filter. Three mL of filtered cells

was collected from the petri dish and delicately layered on top of 2 mL of Histopaque-1077 (Sigma, density: 1.077) in a 15 mL conical tube and centrifuged in a swinging bucket for 35 min at 416 *g* at 32°C. A Polysucrose™ density gradient centrifugation was used to remove small red cells and debris. After centrifugation, the cloud of cells in the interface was collected, adjusted to a final volume of 4 mL, and washed twice with PBS. These freshly collected splenocytes were counted and plated in 35-mm petri dishes at a concentration of 20–30 × 10^6 cells/mL. The medium was RPMI, enriched in GM-CSF, and containing 10% FCS, 2 mM glutamine, 15 mM HEPES pH7.4, 0.2% $NaHCO_3$, penicillin (100 units/mL), and streptomycin (100 µg/mL).

Ethynyl-2′-deoxyuridine staining using click chemistry for cell cycle analysis

Once in the incubator at 4% CO_2 and 37°C, the splenocytes were treated with 10 µM EdU (Santa Cruz Biotechnology) for 60 min. Cells were then collected, washed with 1% BSA-PBS, and fixed in 4% paraformaldehyde in PBS for 15 min at ambient temperature. Fixed cells were permeabilized with 0.5% Triton X-100 in 1% BSA-PBS at ambient temperature for 15 min, centrifuged, then washed once with 1% BSA-PBS, and centrifuged again before labelling. For EdU detection, samples were incubated in PBS with 1 mM $CuSO_4$, 1 µM Alexa 647-azide (Life Technologies), and 100 mM freshly made ascorbic acid for 30 min at ambient temperature in the dark [48]. Cells were washed and resuspended in 200 µL of PBS, 1% BSA, 0.5% Triton X-100 containing 100 µg/mL RNAse (Promega) and 1 µg/mL DAPI (Life Technologies) overnight at 4°C in the dark. On the following day, the cells were washed, resuspended in 500 µL of PBS, 1% BSA, 0.5% Triton X-100. Data were collected with an Attune NxT Flow cytometer and analysed with FlowJo software. For control samples we did not add EdU *ex vivo* and used this as the threshold of detection for EdU [49].

Cell culture, transfections, and protein extracts

HEK 293 cells (American Type Culture Collection CRL-3216) were maintained in DMEM medium supplemented with 10% foetal bovine serum, penicillin (100 units/mL), and streptomycin (100 µg/mL). Transient transfection of 2 × 10^6 cells seeded in a 100-mm plate with different mouse *Zfp36l2* plasmids was performed using Lipofectamine 2000 (Life Technologies) according to the manufacturer's protocol [33]. The transfection mixture containing 1 ug of DNA for each construct was incubated with the cells for 12–18 h and then replaced with fresh medium for a further 24-h incubation, after which the cells were lysed for protein extraction.

Immunoblot analysis

Protein samples were quantitated by Bradford assay (Bio-Rad). Five µg of protein per lane was loaded on a 10% Tris-Glycine polyacrylamide gel and electrophoresed under denaturing conditions. The proteins were transferred from the gel to a nitrocellulose membrane using the Trans-Blot® TurboTM System (Bio-Rad). The membrane was blocked for 1 h with 5% non-fat milk (w/v) in a Tris-buffered saline solution containing 0.1% TWEEN (TBS-T). The following primary antibodies were used for protein detection: mouse monoclonal anti-GFP (Abcam #AB290), dilution 1/1000. The HRP-conjugated secondary antibodies were anti-mouse (Gena-N931V), dilution 1/5000. The HRP signal was developed using the Bio-Rad Western Clarity TM chemiluminescent substrate.

Preparation of RNA probe for RNA electrophoretic mobility assay

An RNA probe was synthesized with the Riboprobe System-T7 (Promega) using DNA primers having sequences immediately downstream from a T7 promoter, as described [50]. The RNA was body-labelled during the transcription process, which was performed in the presence of [α-^{32}P] UTP (3000 Ci/mmol; PerkinElmer). The probe was designed to be ~30 nucleotides when we considered the location of the ARE motif. The synthesized RNA probe was separated from the free nucleotides using Sephadex G50 columns (GE Healthcare Life Sciences) and electrophoresed on a 16% polyacrylamide urea gel. The probe was purified from excised gel fragments after detection by autoradiography, as described [29]. The amount of RNA probe used in each EMSA sample was calculated to be ~10 femtomoles. The sequence of the RNA probe contained a single ARE of the 7-mer type (AUAAUAU) from the 3' UTR of *Apol11b*. The corresponding sequence was *Apol11b*: 5'- AAUGUCAGAAAUAUUUAUUUUCUUGAAGA – 3'.

RNA electrophoretic mobility assay

HEK 293T cells were transiently transfected with wild type mZfp36l2 (WT-L2), mouse Zfp36l2-C175S (disruption of the first zinc finger domain), ZFP36-family members fused to GFP [32], or GFP vector plasmids. Then, protein extracts were prepared as described [29]. The protein extracts were incubated for 15 min at ambient temperature with 0.2×10^5 cpm of ^{32}P-labelled RNA probe in a final volume of 20 µL containing 10 mM HEPES (pH 7.6), 40 mM KCl, 3 mM $MgCl_2$, 0.5 µg/µL heparin, and 60 ng/uL yeast tRNA, as described [29]. The resultant mixtures were applied to 6% nondenaturing acrylamide (37.5:1) gels and subjected to electrophoresis at 150 V for 15 min followed by electrophoresis at 200 V for 90 min in 0.4× Tris-borate/EDTA running buffer. The gels were dried, exposed to film (Carestream BIOMAX MR Film), and developed after 12–20 h of exposure. Each gel shift assay was repeated three times, using different protein extracts to ensure rigour and reproducibility.

Cell culture, UV crosslinking, and eClip

MLTC-1 cells (American Type Culture Collection, CRL 2065) were cultured in RPMI medium with 10% foetal bovine serum, penicillin (100 units/ml), and streptomycin (100 µg/ml), at 37°C in an incubator with 5% CO_2 in atmospheric air. MLTC-1 cells are derived from murine Leydig tumour cells, in which we have previously shown high expression of ZFP36L2 in Westen blots [33]. MLTC-1 cells at 70–80% confluency from a 100-mm petri dish were trypsinized, washed in cold PBS twice, counted and adjusted to 20×10^6 cells/ml. A total of 80×10^6 cells were resuspended in 4 mL of PBS and placed in a clean 100-mm petri dish, on top of an ice plate, inside the UV crosslinker (Hoefer UVC 500 crosslinker). The distance from the 254-nm UV bulbs to the cells was 11 cm. Then, the cells were exposed to 254-nm light with an energy setting of 400 mJoules/cm^2. After UV crosslinking, cells were washed in PBS, counted again, and pelleted (20×10^6 cells) in an Eppendorf tube and snap frozen. Enhanced Crosslinking and Immunoprecipitation (eCLIP) was performed by EclipseBio BioInnovations Inc (San Diego; https://www.eclipsebio.com/) according to [51] protocol. In short, total RNA was extracted from the frozen pellets of MLTC-1 cells after UV-crosslinking, quantified, and analysed for quality using an Agilent 4200TapeStation. Twenty ug of RNA with a RIN of 8.35 was used for immunoprecipitation with the validated Abcam ab70775 antibody. As a negative control, we used a rabbit IgG (ab313801 from Abcam). Following the immunoprecipitation, the samples were treated with proteinase K. The IP-RNA was first fragmented and then used to create a library using an RNA adapter on the 3' end of the target RNA. The RNA was reverse transcribed resulting in cDNAs ligated to single-stranded DNA adapters on the 3' end to serve as identifiers against PCR duplicates. Finally, the paired-end cDNA fragments were amplified to obtain sufficient material for high-throughput sequencing.

eCLIP analysis

The CLIPper algorithm [52] was used to identify RBP-binding peaks. This method calculates significant read clusters relative to gene-level read distribution and length, then filters false positives by requiring a substantial IP/input library fold-change enrichment (we used $\log_2 \geq 3$). Two thousand one hundred and forty-three eCLIP sequences were identified with $\log_2$(Fold Change) >1 and $\log_{10}$(p) <1. These peaks mapped to 597 different genes. For the flanking motif analysis around the AREs we started with all 2,143 reproducible eCLIP peaks, then filtered to those with positive ARE scores, resulting in 320 eCLIP peaks. From these 320 peaks, we extracted 800 WUUUW motif instances (with 10nt flanks) for the Logomaker visualization. A standard motif analysis for RBPs in our eCLIP peaks was initially performed by EclipseBio and did not identify any known motifs commonly attributed to RBPs. Thus, we performed a more advanced *de novo* motif analysis using HOMER v.5.1 (Hypergeometric Optimization of Motif EnRichment). For our HOMER analysis we used 2,143 reproducible (peaks present in both experimental replicate) and filtered for the peaks that were located only at the 3' UTRs, which resulted in 258 peaks. Using these 258 peaks we run HOMER to identify potential novel motifs bound to ZFP36L2. As a background control we used other 7,308 non-reproducible eCLIP peaks (i.e. 3'UTR peaks that did not overlap with the reproducible peaks).

Statistical calculations

Traditional two-tailed t-test was used in most analysis, except for Supplementary Figure S4, when the Welch's two-sample t-test was used to compare mean expression levels between WT and KO samples, because it assumes the expression levels are approximately normally distributed but allow for unequal variances in different tissues, which was the case. p values are *<0.05, **<0.005, ***<0.0005 and ****<0.00005, respectively.

Acknowledgments

We thank Theresa Pratt, Colony Management Support Technician, for animal husbandry and breeding support. We thank Abegael Johnson for assistance in using FlowJo program to analyze cell cycle data. We appreciate Dr. Howard M. Fried for editing the initial version of this manuscript.

GSS, AL, and SBVR conceptualized the body of work and interpreted results. GSS conducted all data analysis and did the code development. DF and JGC contributed with materials, protocols and interpretation for cell cycle experiments. SBVR performed RNA-seq, cell cycle, EMSA and eCLIP experiments, participate on the data analysis, interpretation and conclusions. AL and SBVR supervised the study. SBVR wrote the paper. All authors revised and approved the final manuscript.

Author contributions

CRediT: **George Stephen Stephenson:** Conceptualization, Data curation, Formal analysis, Investigation, Methodology, Software, Visualization; **Dalia Fleifel:** Investigation, Methodology, Resources; **Jeanette Gowen Cook:** Investigation, Methodology, Resources, Supervision; **Alain Laederach:** Conceptualization, Data curation, Funding acquisition, Investigation, Methodology, Resources, Software, Supervision, Visualization, Writing – review & editing; **Silvia Beatriz Vieira Ramos:** Conceptualization, Data curation, Formal analysis, Funding acquisition, Investigation, Methodology, Project administration, Resources, Supervision, Validation, Visualization, Writing – original draft, Writing – review & editing.

Disclosure statement

The authors declare no financial and non-financial competing interest.

Funding

National Institutes of Health [R01 HL111527 to A.L. and S.B.V.R., R35 GM140844 to A.L., R35 GM141833 to J.G.C.]; Office of Research Technologies, UNC Chapel Hill School of Medicine to S.B.V.R. American Heart Association 23PRE1027147 to D.F. The UNC Flow Cytometry Core Facility (RRID:SCR_019170) is supported in part by P30 CA016086 Cancer Center Core Support Grant to the UNC Lineberger Comprehensive Cancer Center.

ORCID

George Stephen Stephenson http://orcid.org/0009-0005-3201-7450
Dalia Fleifel http://orcid.org/0000-0002-6475-8756
Jeanette Gowen Cook http://orcid.org/0000-0003-0849-7405
Alain Laederach http://orcid.org/0000-0002-5088-9907
Silvia Beatriz Vieira Ramos http://orcid.org/0000-0001-7900-9806

Data availability

The datasets generated and/or analysed during the current study are available in the GEO Accession ID. For the differential expression results and RNA-seq reads are provided in the gene expression omnibus (GSE283043). And for the eClip data are provided in (GSE283044). Additional information for the eCLIP peaks can be found in the link below https://genome.ucsc.edu/s/gsgeorge/Zfp36l2_mm10_eclip_peaks.

Ethics approval

The present study uses a mouse model created at UNC. All animal experimentation described here was approved by the Institutional Animal Care and Use Committee of the University of North Carolina approved (IACUC ID# 24-004).

References

[1] Wilson GM, Lu J, Sutphen K, et al. Phosphorylation of p40AUF1 regulates binding to a + U-rich mRNA-destabilizing elements and protein-induced changes in ribonucleoprotein structure. J Biol Chem. 2003;278(35):33039–33048. doi: 10.1074/jbc.M305775200
[2] Cook KB, Kazan H, Zuberi K, et al. Rbpdb: a database of RNA-binding specificities. Nucleic Acids Res. 2011;39 (Database):D301–D308. doi: 10.1093/nar/gkq1069
[3] Fu M, Blackshear PJ. Rna-binding proteins in immune regulation: a focus on CCCH zinc finger proteins. Nat Rev Immunol. 2017;17(2):130–143. doi: 10.1038/nri.2016.129
[4] Hinman MN, Lou H. Diverse molecular functions of Hu proteins. Cell Mol Life Sci. 2008;65(20):3168–3181. doi: 10.1007/s00018-008-8252-6
[5] Caput D, Beutler B, Hartog K, et al. Identification of a common nucleotide sequence in the 3'-untranslated region of mRNA molecules specifying inflammatory mediators. Proc Natl Acad Sci U S A. 1986;83(6):1670–1674. doi: 10.1073/pnas.83.6.1670
[6] Shaw G, Kamen R. A conserved AU sequence from the 3′ untranslated region of GM-CSF mRNA mediates selective mRNA degradation. Cell. 1986;46(5):659–667. doi: 10.1016/0092-8674(86)90341-7
[7] Bakheet T, Frevel M, Williams BR, et al. Ared: human AU-rich element-containing mRNA database reveals an unexpectedly diverse functional repertoire of encoded proteins. Nucleic Acids Res. 2001;29(1):246–254. doi: 10.1093/nar/29.1.246
[8] Xu N, Chen CY, Shyu AB. Modulation of the fate of cytoplasmic mRNA by AU-rich elements: key sequence features controlling mRNA deadenylation and decay. Mol Cell Biol. 1997;17(8):4611–4621. doi: 10.1128/MCB.17.8.4611
[9] Blackshear PJ. Tristetraprolin and other CCCH tandem zinc-finger proteins in the regulation of mRNA turnover. Biochem Soc Trans. 2002;30(6):945–952. doi: 10.1042/bst0300945
[10] Sandler H, Kreth J, Timmers HT, et al. Not1 mediates recruitment of the deadenylase Caf1 to mRNAs targeted for degradation by tristetraprolin. Nucleic Acids Res. 2011;39(10):4373–4386. doi: 10.1093/nar/gkr011
[11] Pekovic F, Lai WS, Corbo J, et al. Multivalent interactions with CCR4-NOT and PABPC1 determine mRNA repression efficiency by tristetraprolin. Nat Commun. 2025;16(1):7528. doi: 10.1038/s41467-025-62741-7
[12] Lykke-Andersen J, Wagner E. Recruitment and activation of mRNA decay enzymes by two ARE-mediated decay activation domains in the proteins TTP and BRF-1. Genes Dev. 2005;19 (3):351–361. doi: 10.1101/gad.1282305
[13] DiTargiani RC, Lee SJ, Wassink S, et al. Functional characterization of iron-substituted tristetraprolin-2D (TTP-2D, NUP475-2D): rNA binding affinity and selectivity. Biochemistry. 2006;45(45):13641–13649. doi: 10.1021/bi060747n
[14] Mukherjee N, Jacobs NC, Hafner M, et al. Global target mRNA specification and regulation by the RNA-binding protein ZFP36. Genome Biol. 2014;15(1):R12. doi: 10.1186/gb-2014-15-1-r12
[15] Cao Y, Huang W, Wu F, et al. Zfp36 protects lungs from intestinal I/R-induced injury and fibrosis through the CREBBP/p53/p21/Bax pathway. Cell Death Dis. 2021;12(7):685. doi: 10.1038/s41419-021-03950-y
[16] Dolicka D, Sobolewski C, Correia de Sousa M, et al. mRNA post-transcriptional regulation by AU-rich element-binding proteins in liver inflammation and cancer. Int J Mol Sci. 2020;21(18):6648. doi: 10.3390/ijms21186648
[17] Guo J, Lei M, Cheng F, et al. Rna-binding proteins tristetraprolin and human antigen R are novel modulators of podocyte injury in diabetic kidney disease. Cell Death Dis. 2020;11(6):413. doi: 10.1038/s41419-020-2630-x
[18] Ramos SB, Stumpo DJ, Kennington EA, et al. The CCCH tandem zinc-finger protein Zfp36l2 is crucial for female fertility and early embryonic development. Development. 2004;131(19):4883–4893. doi: 10.1242/dev.01336
[19] Redmon IC, Ardizzone M, Hekimoglu H, et al. Sequence and tissue targeting specificity of ZFP36L2 reveals Elavl2 as a novel target with co-regulation potential. Nucleic Acids Res. 2022;50(7):4068–4082. doi: 10.1093/nar/gkac209

[20] Stumpo DJ, Broxmeyer HE, Ward T, et al. Targeted disruption of Zfp36l2, encoding a CCCH tandem zinc finger RNA-binding protein, results in defective hematopoiesis. Blood. 2009;114(12):2401–2410. doi: 10.1182/blood-2009-04-214619
[21] Zheng W, Sha QQ, Hu H, et al. Biallelic variants in ZFP36L2 cause female infertility characterised by recurrent preimplantation embryo arrest. J Med Genet. 2022;59(9):850–857. doi: 10.1136/jmedgenet-2021-107933
[22] Iwanaga E, Nanri T, Mitsuya H, et al. Mutation in the RNA binding protein TIS11D/ZFP36L2 is associated with the pathogenesis of acute leukemia. Int J Oncol. 2011;38(1):25–31. doi: 10.3892/ijo_00000820
[23] Podszywalow-Bartnicka P, Neugebauer KM. Multiple roles for AU-rich RNA binding proteins in the development of haematologic malignancies and their resistance to chemotherapy. RNA Biol. 2024;21(1):584–600. doi: 10.1080/15476286.2024.2346688
[24] Zhang L, Prak L, Rayon-Estrada V, et al. Zfp36l2 is required for self-renewal of early burst-forming unit erythroid progenitors. Nature. 2013;499(7456):92–96. doi: 10.1038/nature12215
[25] Chousal J, Cho K, Ramaiah M, et al. Chromatin modification and global transcriptional silencing in the oocyte mediated by the mRNA decay activator ZFP36L2. Dev Cell. 2018;44(3):392–402.e7.
[26] Makita S, Takatori H, Iwata A, et al. Rna-binding protein ZFP36L2 downregulates helios expression and suppresses the function of regulatory T cells. Front Immunol. 2020;11:1291. doi: 10.3389/fimmu.2020.01291
[27] Wang E, Zhou H, Nadorp B, et al. Surface antigen-guided CRISPR screens identify regulators of myeloid leukemia differentiation. Cell STEM Cell. 2021;28(4):718–731.e6. doi: 10.1016/j.stem.2020.12.005
[28] Shen L. GeneOverlap: test and visualize gene overlaps [Internet]. R package version 1.49.0. 2026. [cited 2026 Jun 19]. Available from: https://bioconductor.org/packages/GeneOverlap
[29] Ball CB, Solem AC, Meganck RM, et al. Impact of RNA structure on ZFP36L2 interaction with luteinizing hormone receptor mRNA. RNA. 2017;23(8):1209–1223. doi: 10.1261/rna.060467.116
[30] Spasic M, Friedel CC, Schott J, et al. Genome-wide assessment of AU-rich elements by the AREScore algorithm. PLOS Genet. 2012;8(1):e1002433. doi: 10.1371/journal.pgen.1002433
[31] Yu B, Shan G. Functions of long noncoding RNAs in the nucleus. Nucleus. 2016;7(2):155–166. doi: 10.1080/19491034.2016.1179408
[32] Phillips RS, Ramos SB, Blackshear PJ. Members of the tristetraprolin family of tandem CCCH zinc finger proteins exhibit CRM1-dependent nucleocytoplasmic shuttling. J Biol Chem. 2002;277(13):11606–11613. doi: 10.1074/jbc.M111457200
[33] Ball CB, Rodriguez KF, Stumpo DJ, et al. The RNA-binding protein, ZFP36L2, influences ovulation and oocyte maturation. PLOS ONE. 2014;9(5):e97324. doi: 10.1371/journal.pone.0097324
[34] Liu C, Peng H, Yu J, et al. Impaired ketogenesis in Leydig cells drives testicular aging. Nat Commun. 2025;16(1):4224. doi: 10.1038/s41467-025-59591-8
[35] Li T, Li S, Chen D, et al. Transcriptomic analyses of RNA-binding proteins reveal eIF3C promotes cell proliferation in hepatocellular carcinoma. Cancer Sci. 2017;108(5):877–885. doi: 10.1111/cas.13209
[36] Assoni G, La Pietra V, Digilio R, et al. HuR-targeted agents: an insight into medicinal chemistry, biophysical, computational studies and pharmacological effects on cancer models. Adv Drug Deliv Rev. 2022;181:114088. doi: 10.1016/j.addr.2021.114088
[37] Ignarski M, Rill C, Kaiser RWJ, et al. The RNA-protein interactome of differentiated kidney tubular epithelial cells. J Am Soc Nephrol. 2019;30(4):564–576. doi: 10.1681/ASN.2018090914
[38] Sidali A, Teotia V, Solaiman NS, et al. Au-rich element RNA binding proteins: at the crossroads of post-transcriptional regulation and genome integrity. Int J Mol Sci. 2021;23(1):96. doi: 10.3390/ijms23010096
[39] Galloway A, Saveliev A, Lukasiak S, et al. Rna-binding proteins ZFP36L1 and ZFP36L2 promote cell quiescence. Science. 2016;352(6284):453–459. doi: 10.1126/science.aad5978
[40] Salerno F, Whale AJ, Matheson LS, et al. RNA binding proteins control the G(2)-M checkpoint of the germinal center B cell. Sci Immunol. 2025;10(112):eadu3718. doi: 10.1126/sciimmunol.adu3718
[41] Murn J, Teplova M, Zarnack K, et al. Recognition of distinct RNA motifs by the clustered CCCH zinc fingers of neuronal protein Unkempt. Nat Struct Mol Biol. 2016;23(1):16–23. doi: 10.1038/nsmb.3140
[42] Shah K, He S, Turner DJ, et al. Regulation by the RNA-binding protein unkempt at its effector interface. Nat Commun. 2024;15(1):3159. doi: 10.1038/s41467-024-47449-4
[43] Lorenz DA, Her HL, Shen KA, et al. Multiplexed transcriptome discovery of RNA-binding protein binding sites by antibody-barcode eCLIP. Nat Methods. 2023;20(1):65–69. doi: 10.1038/s41592-022-01708-8
[44] Schwarzl T, Sahadevan S, Lang B, et al. Improved discovery of RNA-binding protein binding sites in eCLIP data using DEWSeq. Nucleic Acids Res. 2024;52(1):e1. doi: 10.1093/nar/gkad998
[45] Corley M, Flynn RA, Lee B, et al. Footprinting SHAPE-eCLIP reveals transcriptome-wide hydrogen bonds at RNA-protein interfaces. Mol Cell. 2020;80(5):903–914.e8. doi: 10.1016/j.molcel.2020.11.014
[46] Ducoli L, Zarnegar BJ, Porter DF, et al. Irclip-RNP and Re-CLIP reveal patterns of dynamic protein assemblies on RNA. Nature. 2025;641(8063):769–778. doi: 10.1038/s41586-025-08787-5
[47] Smedley D, Haider S, Ballester B, et al. Biomart–biological queries made easy. BMC Genomics. 2009;10(1):22. doi: 10.1186/1471-2164-10-22

[48] Salic A, Mitchison TJ. A chemical method for fast and sensitive detection of DNA synthesis in vivo. Proc Natl Acad Sci U S A. 2008;105(7):2415–2420. doi: 10.1073/pnas.0712168105
[49] Matson JP, Dumitru R, Coryell P, et al. Rapid DNA replication origin licensing protects stem cell pluripotency. Elife. 2017;6. doi: 10.7554/eLife.30473
[50] Milligan JF, Groebe DR, Witherell GW, et al. Oligoribonucleotide synthesis using T7 RNA polymerase and synthetic DNA templates. Nucl Acids Res. 1987;15(21):8783–8798. doi: 10.1093/nar/15.21.8783
[51] Van Nostra Nd EL, Pratt GA, Shishkin AA, et al. Robust transcriptome-wide discovery of RNA-binding protein binding sites with enhanced CLIP (eCLIP). Nat Methods. 2016;13(6):508–514. doi: 10.1038/nmeth.3810
[52] Lovci MT, Ghanem D, Marr H, et al. Rbfox proteins regulate alternative mRNA splicing through evolutionarily conserved RNA bridges. Nat Struct Mol Biol. 2013;20(12):1434–1442. doi: 10.1038/nsmb.2699